Open Access

Journal of Energy and Power Technology

LIDSEN Publishing Inc.

Original Research

Nonlinear Optimal Control for Six-Phase Induction Generator-Based Renewable Energy Systems

Gerasimos Rigatos [1, *], Masoud Abbaszadeh [2], Bilal Sari [3], Pierluigi Siano [4]

1. Unit of Industrial Automation Industrial Systems Institute 26504, Rion Patras, Greece; E-Mail: grigat@ieee.org
2. Dept. ECS Engineering Rensselaer Polytechnic Inst. 12065, New York, USA; E-Mail: masouda@ualberta.ca
3. Dept. of Electrical Eng. University of Setif I Setif, 19000, Algeria; E-Mail: bilal.sari@univ-setif.dz
4. Dept. of Innovation Syst. University of Salerno 84084, Fisciano, Italy; E-Mail: psiano@unisa.it

* **Correspondence:** Gerasimos Rigatos; E-Mail: grigat@ieee.org

Academic Editor: Mohammad Jafari

Special Issue: Optimal Energy Management and Control of Renewable Energy Systems

Journal of Energy and Power Technology
2023, volume 5, issue 2
doi:10.21926/jept.2302018

Received: December 07, 2022
Accepted: May 04, 2023
Published: May 11, 2023

Abstract

The article aims at optimizing six-phase induction generator-based renewable energy systems (6-phase IGs or dual star induction generators) through a novel nonlinear optimal control method. Six-phase induction generators appear to be advantageous compared to three-phase synchronous or asynchronous power generators, in terms of fault tolerance and improved power generation rates. The dynamic model of the six-phase induction generator is first written in a nonlinear and multivariable state-space form. It is proven that this model is differentially flat. The 6-phase IG is approximately linearized around a temporary operating point recomputed at each sampling interval to design the optimal controller. The linearization is based on first-order Taylor series expansion and the Jacobian matrices of the state-space model of the 6-phase IG. A stabilizing optimal (H-infinity) feedback controller is designed for the linearized state-space description of the six-phase IG. The feedback gains of the controller are computed by solving an algebraic Riccati equation at each iteration of the control method.

Lyapunov analysis is used to demonstrate global stability for the control loop. The H-infinity Kalman Filter is also used as a robust state estimator, which allows for implementing sensorless control for 6-phase IG-based renewable energy systems. The nonlinear optimal control method achieves fast and accurate tracking of setpoints by the state variables of the 6-phase IG, under moderate variations of the control inputs.

Keywords
Renewable energy systems; six-phase induction generator; nonlinear H-infinity control; Taylor series expansion; Jacobian matrices; Riccati equation; global stability; differential flatness properties

1. Introduction

Multi-phase generators exhibit specific advantages when compared to three-phase synchronous or asynchronous generators as parts of renewable energy systems (for instance wind power generation units or marine/tidal power generation units) [1-4]. In particular 6-phase dual star induction generators (DSIGs) consist of dual 3-phase windings in their stator, and can achieve better power rates [5-9]. Besides, they exhibit fault tolerance and remain functional when one or more of their phases undergo a failure [10-12]. Models of six-phase induction generators combine the rotor's turn motion with the electrical dynamics of the stator's and rotor's phases [13-17]. To integrate 6-phase dual star induction generators in the main electricity grid, two three-phase AC/DC converters can be used, each connected with one of the stator's three-phase windings [18-20]. Due to the nonlinearities and multivariable structure of the associated state-space model the control and stabilization problem of 6-phase DSIGs is nontrivial [21-24]. Several attempts have been made to develop model-based control schemes for 6-phase DSIGs and to demonstrate robustness of the associated control loops to model uncertainty and perturbations [25-28]. In particular results on sliding-mode-type and fault-tolerant control of six-phase induction generators can be found in [29-31]. Moreover, there have been some efforts to implement model-free control based on PID and fuzzy logic control concepts [32-34]. However, little has been done to treat the nonlinear optimal control problem for 6-phase DSIGs.

In the present article a novel nonlinear optimal control method is developed for 6-phase dual star induction generators. Using Kirchhoff's equations in the windings of the stator and rotor of the DSIG the state-space model of the six-phase induction generator is obtained. It is also demonstrated that this model is differentially flat, which is implicit proof of the controllability of the DSIG. Next, to apply the proposed nonlinear optimal control method, the dynamic model of the DSIG undergoes approximate linearization through first-order Taylor series expansion and the computation of the associated Jacobian matrices [35-37]. The linearization process takes place at each sampling instance around a temporary operating point which is defined by the present value of the system's state vector and by the last sampled value of the control inputs vector. The modelling error due to the truncation of higher-order terms from the Taylor series is considered a perturbation that is asymptotically compensated by the robustness of the control algorithm. A stabilizing H-infinity feedback controller is designed for the approximately linearized model of the 6-phase DSIG.

The H-infinity controller of the DSIG offers a solution to the associated nonlinear optimal control problem under model uncertainty and external perturbations. It represents a min-max differential game taking place between (i) the control inputs which try to minimize a quadratic cost function of the state vector's tracking error (ii) the model imprecision and exogenous perturbations which try to maximize this cost function. To select the stabilizing feedback gains of the H-infinity controller an algebraic Riccati equation is solved at each iteration of the control algorithm [38-41]. The global stability properties of the control method are proven through Lyapunov analysis. First, it is demonstrated that the control loop satisfies the H-infinity tracking performance criterion which signifies robustness [42, 43]. Next, under moderate conditions, it is also proven that the control loop is globally asymptotically stable [38-41]. The H-infinity Kalman Filter is used as a robust state estimator to enable state estimation-based control without the need to measure the entire state vector of the DSIG. The nonlinear optimal control method achieves fast and accurate tracking of setpoints by all state variables of the DSIG. Moreover, it enables the minimization of the control input's variations, thus reducing energy dispersion during the functioning of the DSIG.

The article's structure is as follows: In Section 2 the dynamic model of the 6-phase DSIG is defined and the associated state-space description in matrix form is formulated. In Section 3 differential flatness properties are proven for the 6-phase DSIG and a flatness-based controller is designed for this power generation system. In Section 4 the state-space model of the DSIG undergoes approximate linearization with the use of Taylor series expansion. In Section 5 an H-infinity feedback controller is designed for the DSIG. In Section 6 the global stability properties of the H-infinity control method for the DSIG are proven through Lyapunov analysis. In Section 7 the performance of the nonlinear optimal control method of the DSIG is tested through simulation experiments. Finally in Section 8 concluding remarks are stated.

2. Dynamic Model of the 6-Phase Dual Star Induction Generator

The considered renewable energy system comprises a wind or a marine turbine connected with a 6-phase dual-star induction generator (6-phase DSIG). Next, two AC/DC converters connect the 6-phase DSIG with the main electricity grid. The diagram of the renewable power generation unit based on a 6-phase dual star induction generator (6-phase DSIG) is shown in Figure 1.

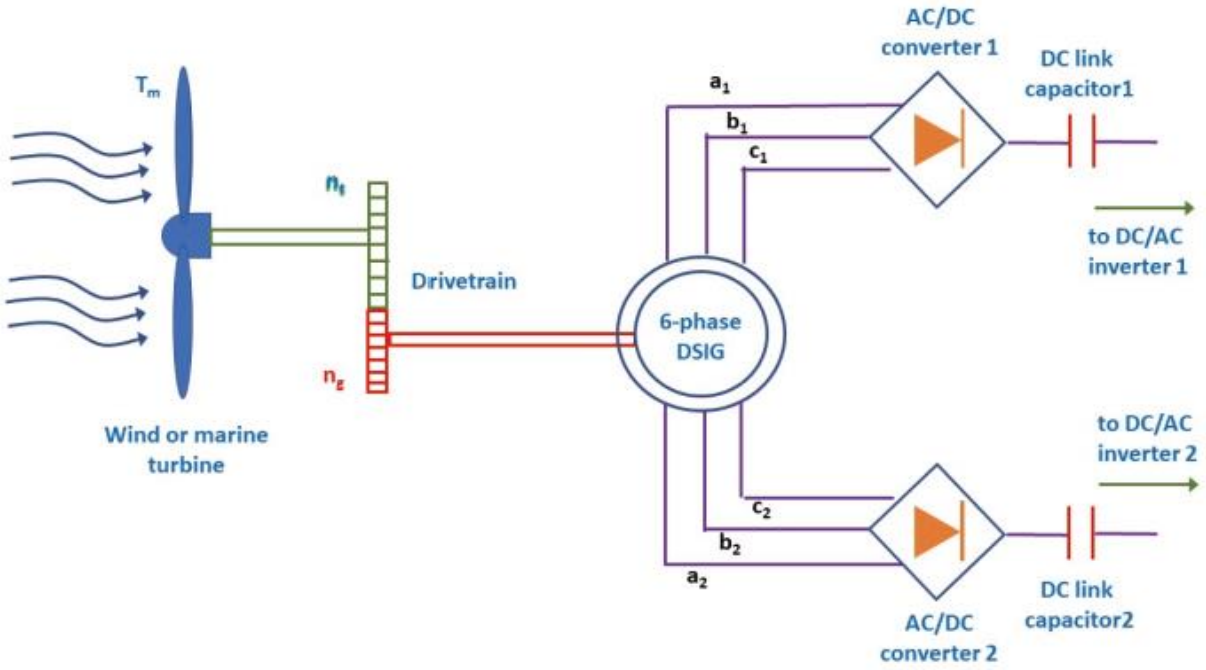

Figure 1 Diagram of a renewable power generation unit which is based on a 6-phase dual star induction generator (6-phase DSIG).

The turn motion of the generator's rotor is given by

$$J\dot{\omega}_g = T_m - T_{em} - b\omega_g \tag{1}$$

where *J* is the moment of inertia of the rotor, ω_g is the rotor's angular speed, T_g is the mechanical torque due to wind and T_{em} is the electromagnetic torque of the generator, and *b* is the friction coefficient. There are two *abc* phase frames and equivalently under the field orientation assumption there are two *dq* reference frames of the stator. The magnetic flux in these frames is denoted by ψ, the current variable is denoted by *i* and the voltage variable is denoted by *V*. The dynamic model of the six-phase induction generator is obtained after applying Kirchhoff's laws in the circuit of the stator and of the rotor.

As noted above, two different *abc* reference frames have been used to describe voltage and current variables in the stator circuits. Next, by applying Clark's transformation the three-phase *abc* frames are turned into *ab* two-phase frames, while by applying Park's transformation the *ab* frames are turned into *dq* asynchronously rotating frames. Thus one has for the stator expression of the current and voltage variables in reference frames dq_{s1} and in reference frame dq_{s2}. Equivalently, the voltage and current variables of the rotor are expressed initially in an *ABC* three-phase reference frame which after applying Clark's and Park's transformations is turned into the asynchronously rotating reference frame dq_r Therefore, one has the following sets of equations [5-9]:

$$V_{ds1} = R_{s1}i_{ds1} + \frac{d}{dt}\psi_{ds1} - \omega_s\psi_{qs1} \tag{2}$$

$$V_{qs1} = R_{s1}i_{qs1} + \frac{d}{dt}\psi_{qs1} + \omega_s\psi_{ds1} \tag{3}$$

$$V_{ds2} = R_{s2}i_{ds2} + \frac{d}{dt}\psi_{ds2} - \omega_s\psi_{qs2} \tag{4}$$

$$V_{qs2} = R_{s2}i_{qs2} + \frac{d}{dt}\psi_{qs2} + \omega_s\psi_{ds2} \tag{5}$$

$$V_{dr} = R_r i_{dr} + \frac{d}{dt}\psi_{dr} - \omega_s\psi_{qr} \tag{6}$$

$$V_{qr} = R_r i_{qr} + \frac{d}{dt}\psi_{qr} + \omega_s\psi_{dr} \tag{7}$$

Moreover, the magnetic flux variables are connected with the stator and rotor current variables through the following equations [5-9].

$$\psi_{ds1} = L_{s1}i_{ds1} + L_m(i_{ds1} + i_{ds2} + i_{dr}) \tag{8}$$

$$\psi_{qs1} = L_{s1}i_{qs1} + L_m\big(i_{qs1} + i_{qs2} + i_{qr}\big) \tag{9}$$

$$\psi_{ds2} = L_{s2}i_{ds2} + L_m(i_{ds1} + i_{ds2} + i_{dr}) \tag{10}$$

$$\psi_{qs2} = L_{s2}i_{qs2} + L_m\big(i_{qs1} + i_{qs2} + i_{qr}\big) \tag{11}$$

$$\psi_{dr} = L_r i_{dr} + L_m(i_{ds1} + i_{ds2} + i_{dr}) \tag{12}$$

$$\psi_{qr} = L_r i_{qr} + L_m\big(i_{qs1} + i_{qs2} + i_{qr}\big) \tag{13}$$

The electromagnetic torque of the generator is given by [5-9].

$$T_{em} = p\frac{L_m}{L_m + L_r}\big[\big(i_{qs1} + i_{qs2}\big)\psi_{dr} - (i_{ds1} + i_{ds2})\psi_{qr}\big] \tag{14}$$

where L_r is the rotor's inductance and L_m is the mutual inductance of the generator. Besides the slip speed of the generator is defined as

$$\omega_{sl} = \omega_s - \omega_r \tag{15}$$

which is the difference between the reference speed ω_s (that is associated with the grid's frequency) and the rotor's speed ω_r (where for a DSIG with $\frac{p}{2}$ pole pairs it holds that its mechanical turn speed ω_m satisfies the relation $\omega_r = \frac{p}{2}\omega_m$.

The diagram of the stator and rotor phase reference frames of the 6-phase dual star induction generator is shown in Figure 2. The stator has two three-phase frames which are denoted as $a_{s1}b_{s1}c_{s1}$ and $a_{s2}b_{s2}c_{s2}$ respectively. The second frame is shifted concerning the first frame by an angle a = 30°. The rotor's three-phase frame is denoted as $a_rb_rc_r$.

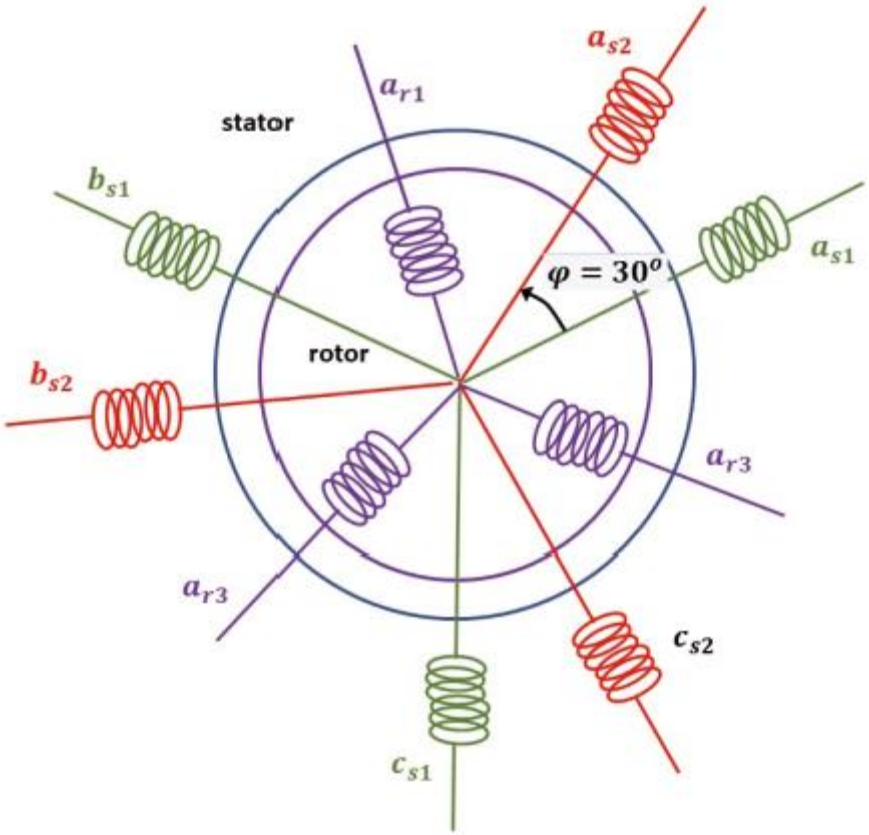

Figure 2 Diagram of the stator and rotor reference frames of the 6-phase dual star induction generator: $a_{s1}b_{s1}c_{s1}$ is the first 3-phase frame of the stator, and $a_{s2}b_{s2}c_{s2}$ is the second 3-phase frame of the stator, while $a_{r1}b_{r1}c_{r1}$ is the 3-phase frame of the rotor.

The active and reactive power of the two frames of the stator is given by $P_s = P_1 + P_2$ and $Q_s = Q_1 + Q_2$, where

$$\begin{aligned} P_1 &= v_{ds1}i_{ds1} + v_{qs1}i_{qs1} \\ Q_1 &= v_{qs1}i_{ds1} - v_{ds1}i_{qs1} \end{aligned} \tag{16}$$

$$\begin{aligned} P_2 &= v_{ds2}i_{ds2} + v_{qs2}i_{qs2} \\ Q_2 &= v_{qs2}i_{ds2} - v_{ds2}i_{qs2} \end{aligned} \tag{17}$$

Next, the field orientation assumption is made about the magnetic flux of the motor (the rotor's *dq* frame turns at an asynchronous speed which allows to set equal to zero the q-axis component of the rotor's magnetic flux). This signifies $\psi_{dr} = \psi_r$ and $\psi_{qr} = 0$ [5-9].

By substituting the above-given field orientation conditions in Eq. (6) and Eq. (7) and using that $V_{dr} = 0$, $V_{qr} = 0$ and $\frac{d}{dt}\psi_r = 0$ one obtains [5-9].

$$0 = R_r i_{dr} + \frac{d}{dt}\psi_{dr} \Rightarrow i_{dr} = 0 \tag{18}$$

$$0 = R_r i_{qr} + \frac{d}{dt}\psi_{qr} + \omega_s \psi_r \Rightarrow i_{qr} = -\frac{\omega_{sl}\psi_r}{R_r} \tag{19}$$

Next, from Eq. (12) and Eq. (13) one has about the rotor currents.

$$\psi_r = (L_r + L_m)i_{dr} + L_m(i_{ds1} + i_{ds2}) \Rightarrow i_{dr} = \frac{L_m}{L_m + L_r}[\psi_r - L_m(i_{ds1} + i_{ds2})] \quad (20)$$

$$0 = (L_r + L_m)i_{qr} + L_m\left(i_{qs1} + i_{qs2}\right) \Rightarrow i_{qr} = -\frac{L_m}{L_m + L_r}\left[\psi_r\left(i_{qs1} + i_{qs2}\right)\right] \quad (21)$$

Moreover, from Eq. (19) and Eq. (21) one obtains.

$$-\frac{\omega_{sl}\psi_r}{R_r} = -\frac{L_m}{L_m + L_r}\left(i_{qs1} + i_{qs2}\right) \Rightarrow \omega_s = -\frac{R_r L_m}{L_m + L_r}\frac{\left(i_{qs1} + i_{qs2}\right)}{\psi_r} \quad (22)$$

Moreover, the relation between the electromagnetic torque of the DSIG becomes.

$$T_{em} = p\frac{L_m}{L_m + L_r}\left[\left(i_{qs1} + i_{qs2}\right)\psi_r\right] \quad (23)$$

Using that $\psi_{dr} = \psi_r$, $\psi_{qr} = 0$ and by substituting Eq. (8)-Eq. (13) into Eq. (2)-Eq. (7) one obtains the following equations about the electrical dynamics of the stator of the DSIG [5-9].

$$V_{ds1} = R_{s1}i_{ds1} + L_{s1}\frac{d}{dt}i_{ds1} - \omega_s\left(L_{s1}i_{qs1} + \frac{L_r}{R_r}\psi_r\omega_s\right) \quad (24)$$

$$V_{qs1} = R_{s1}i_{qs1} + L_{s1}\frac{d}{dt}i_{qs1} + \omega_s(L_{s1}i_{ds1} + \psi_r) \quad (25)$$

$$V_{ds2} = R_{s2}i_{ds2} + L_{s2}\frac{d}{dt}i_{ds2} - \omega_s\left(L_{s2}i_{qs2} + \frac{L_r}{R_r}\psi_r\omega_s\right) \quad (26)$$

$$V_{qs2} = R_{s2}i_{qs2} + L_{s2}\frac{d}{dt}i_{qs2} + \omega_s(L_{s2}i_{ds2} + \psi_r) \quad (27)$$

Moreover, using that $\frac{L_r}{R_r}\psi_r\omega_s = \frac{L_r L_m}{L_r + L_m}(i_{qs1} + i_{qs2})$ the integrated dynamics of the 6-phase dual star induction generator becomes [5-9].

$$\frac{d}{dt}\omega_g = \frac{1}{J}\left[p\frac{L_m}{L_m + L_r}\left(i_{qs1} + i_{qs2}\right)\psi_r - T_m - b\omega_g\right] \quad (28)$$

$$\frac{d}{dt}\psi_r = -\frac{R_r}{L_r + L_m}\psi_r + \frac{R_r L_m}{L_m + L_r}(i_{ds1} + i_{ds2}) \quad (29)$$

$$\frac{d}{dt}i_{ds1} = \frac{1}{L_{s1}}\left\{-R_{s1}i_{ds1} + \omega_s\left(L_{s1}i_{qs1} + \frac{L_r L_m}{L_r + L_m}\left(i_{qs1} + i_{qs2}\right) + V_{ds1}\right)\right\} \quad (30)$$

$$\frac{d}{dt}i_{qs1} = \frac{1}{L_{s1}}\left\{-R_{s1}i_{qs1} - \omega_s\left(L_{s1}i_{ds1+\psi_r} + V_{qs1}\right)\right\} \quad (31)$$

$$\frac{d}{dt}i_{ds2} = \frac{1}{L_{s2}}\left\{-R_{s2}i_{ds2} + \omega_s\left(L_{s2}i_{qs2} + \frac{L_r L_m}{L_r + L_m}\left(i_{qs1} + i_{qs2}\right) + V_{ds2}\right)\right\} \quad (32)$$

$$\frac{d}{dt}i_{qs2} = \frac{1}{L_{s2}}\{-R_{s2}i_{qs2} - \omega_s(L_{s2}i_{ds2+\psi_r} + V_{qs2})\} \tag{33}$$

Next, by defining the state vector.

$$x = [x_1, x_2, x_3, x_4, x_5, x_6]^T \Rightarrow x = \left[\omega_g, \psi_r, i_{ds1}, i_{qs1}, i_{ds2}, i_{qs2}\right]^T \tag{34}$$

and the control inputs vector.

$$u = [u_1, u_2, u_3, u_4]^T = \left[V_{ds1}, V_{qs1}, V_{ds2}, V_{qs2}\right]^T \tag{35}$$

one obtains the following state-space description of the DSIG.

$$\frac{d}{dt}x_1 = \frac{1}{J}\left[p\frac{L_m}{L_m + L_r}(x_4 + x_6)x_2 - T_m - bx_1\right] \tag{36}$$

$$\frac{d}{dt}x_2 = \frac{R_r}{L_r + L_m}x_2 + \frac{R_r L_m}{L_m + L_r}(x_3 + x_5) \tag{37}$$

$$\frac{d}{dt}x_3 = \frac{1}{L_{s1}}\left\{-R_{s1}x_3 + \omega_s\left(L_{s1}x_4 + \frac{L_r L_m}{L_r + L_m}(x_4 + x_6) + u_1\right)\right\} \tag{38}$$

$$\frac{d}{dt}x_4 = \frac{1}{L_{s1}}\{-R_{s1}x_4 - \omega_s(L_{s1}x_3 + x_2) + u_2)\} \tag{39}$$

$$\frac{d}{dt}x_5 = \frac{1}{L_{s2}}\left\{-R_{s2}x_5 + \omega_s\left(L_{s2}x_6 + \frac{L_r L_m}{L_r + L_m}(x_4 + x_6) + u_3\right)\right\} \tag{40}$$

$$\frac{d}{dt}x_6 = \frac{1}{L_{s2}}\{-R_{s2}x_6 - \omega_s(L_{s2}x_5 + x_2) + u_4\} \tag{41}$$

Finally. one obtains a description of the dynamics of the 6-phase DSIG in the following matrix form.

$$\begin{pmatrix}\dot{x}_1\\ \dot{x}_2\\ \dot{x}_3\\ \dot{x}_4\\ \dot{x}_5\\ \dot{x}_6\end{pmatrix} = \begin{pmatrix} \frac{1}{J}\left[p\frac{L_m}{L_m + L_r}(x_4 + x_6)x_2 - T_m - bx_1\right] \\ -\frac{R_r}{L_r + L_m}x_2 + \frac{R_r L_m}{L_m + L_r}(x_3 + x_5) \\ \frac{1}{L_{s1}}\left\{-R_{s1}x_3 + \omega_s\left(L_{s1}x_4 + \frac{L_r L_m}{L_r + L_m}(x_4 + x_6)\right)\right\} \\ \frac{1}{L_{s1}}\{-R_{s1}x_4 - \omega_s(L_{s1}x_3 + x_2))\} \\ \frac{1}{L_{s2}}\left\{-R_{s2}x_5 + \omega_s\left(L_{s2}x_6 + \frac{L_r L_m}{L_r + L_m}(x_4 + x_6)\right)\right\} \\ \frac{1}{L_{s2}}\{-R_{s2}x_6 - \omega_s(L_{s2}x_5 + x_2)\} \end{pmatrix} + \begin{pmatrix} 0 & 0 & 0 & 0 \\ 0 & 0 & 0 & 0 \\ \frac{\omega_s}{L_{s1}} & 0 & 0 & 0 \\ 0 & -\frac{\omega_s}{L_{s1}} & 0 & 0 \\ 0 & 0 & \frac{\omega_s}{L_{s2}} & 0 \\ 0 & 0 & 0 & -\frac{\omega_s}{L_{s2}} \end{pmatrix}\begin{pmatrix}u_1\\ u_2\\ u_3\\ u_4\end{pmatrix} \tag{42}$$

Consequently, the linearized model of the six-phase induction generator can be written in the nonlinear affine-in-the-input state-space form.

$$\dot{x} = f(x) + g(x)u \tag{43}$$

where $x \in R^{6\times 1}$, $f(x) \in R^{6\times 1}$, $g(x) \in R^{6\times 4}$ and $u \in R^{4\times 1}$. The main parameters of the dynamic model of the six-phase induction generator are outline in Table 1.

Table 1 Parameters of the six-phase induction generator model.

Parameter	Definition
J	moment of inertia of the rotor
ω_g	rotor's angular speed
T_g	mechanical torque due to wind
T_{em}	electromagnetic torque of the rotor
V_{ds1}, i_{ds1}	d-axis components of voltage, current at stator frame 1
V_{qs1}, i_{qs1}	q-axis components of voltage, current at stator frame 1
V_{ds1}, i_{ds1}	d-axis components of voltage, current at stator frame 2
V_{qs1}, i_{qs1}	q-axis components of voltage, current at stator frame 2
V_{dr}, i_{dr}	d-axis components of voltage, current at rotor frame
V_{qr}, i_{qr}	q-axis components of voltage, current at rotor frame
ψ_{ds1}, ψ_{qs1}	dq-axis components of magnetic flux at stator frame 1
ψ_{ds2}, ψ_{qs2}	dq-axis components of magnetic flux at stator frame 2
ψd_r, ψ_{qr}	dq-axis components of magnetic flux at rotor frame
R_{s1}, R_{s2}	resistance of stator windings at frames 1 and 2
L_{s1}, L_{s2}	inductance of stator windings at frames 1 and 2
P_1, Q_1	active and reactive power at stator windings frames 1
P_2, Q_2	active and reactive power at stator windings frames 2
R_r	resistance of rotor windings
L_r	inductance of rotor windings
L_m	mutual inductance between stator and rotor
ω_s	frequency of the electric grid

3. Differential Flatness Properties of the 6-Phase Dual Star Induction Generator

3.1 Proof of Differential Flatness Properties

It will be proven that the dynamic model of the 6-phase DSIG is differentially flat, with flat outputs vector.

$$Y = [Y_1, Y_2, Y_3, Y_4]^T \Rightarrow Y = \left[\omega_g, \psi_r, i_{d_s}, i_{q_s}\right]^T \Rightarrow Y = [x_1, x_2, x_3, x_4]^T \tag{44}$$

Indeed from the first state-space equation of the DSIG given in Eq. (36) and by assuming that the mechanical torque T_m which is generated by the wind or the tidal stream is piecewise constant, one has

$$x_6 = \frac{J\dot{x}_1 - \frac{pL_m}{L_m + L_r} x_2 x_4 + T_m + bx_1}{\frac{pL_m}{L_m + L_r} x_2} \Rightarrow x_6 = h_6(Y, \dot{Y}) \tag{45}$$

which signifies that state variable x_6 is a differential function of the flat outputs vector of the system. Next, from the second state-space equation of the DSIG given in Eq. (37) one obtains

$$x_5 = \frac{\dot{x}_2 - \frac{R_r}{L_m + L_r} x_2 - \frac{R_r L_m}{L_m + L_r} x_3}{\frac{R_r L_m}{L_m + L_r}} \Rightarrow x_5 = h_5(Y, \dot{Y}) \tag{46}$$

which signifies that state variable x_5 is a differential function of the flat outputs of the system. Moreover, from Eq. (38) to Rq. (41) one has

$$\begin{pmatrix} u_1 \\ u_2 \\ u_3 \\ u_4 \end{pmatrix} = \begin{pmatrix} \frac{\omega_s}{L_s} & 0 & 0 & 0 \\ 0 & -\frac{\omega_s}{L_s} & 0 & 0 \\ 0 & 0 & \frac{\omega_s}{L_s} & 0 \\ 0 & 0 & 0 & -\frac{\omega_s}{L_s} \end{pmatrix}^{-1} \left[\begin{pmatrix} \dot{x}_3 \\ \dot{x}_4 \\ \dot{x}_5 \\ \dot{x}_6 \end{pmatrix} - \begin{pmatrix} \frac{1}{L_{s1}} \left\{ -R_{s1} x_3 + \omega_s \left(L_{s1} x_4 + \frac{L_r L_m}{L_r + L_m} (x_4 + x_6) \right) \right\} \\ \frac{1}{L_{s1}} \{ -R_{s1} x_4 - \omega_s (L_{s1} x_3 + x_2) \} \\ \frac{1}{L_{s2}} \left\{ -R_{s2} x_5 + \omega_s \left(L_{s2} x_6 + \frac{L_r L_m}{L_r + L_m} (x_4 + x_6) \right) \right\} \\ \frac{d}{dt} x_6 = \frac{1}{L_{s2}} \{ -R_{s2} x_6 - \omega_s (L_{s2} x_5 + x_2) \} \end{pmatrix} \right] \tag{47}$$

Eq. (47) shows that the control inputs of the 6-phase DSIG can also be written as differential functions of the flat outputs vector of the system. Thus, by demonstrating that the state variables of the 6-phase DSIG x_1 to x_6 and the control inputs u_1 to u_4 are differential functions of the flat outputs vector, it can be concluded that this system is differentially flat.

The differential flatness property of the 6-phase DSIG signifies that the system is input-output linearizable. It is also an implicit proof of the system's controllability. Moreover, it also allows for solving the setpoints definition problem in the associated control loop. First, one defines setpoints in an unconstraint manner for the four state-vector elements of the DSIG x_1 to x_4 which are also flat outputs of the system. Next, one defines setpoints for state variables x_5 and x_6, under the constraint that these terms are differential functions of the flat outputs of the system.

Indeed, based on successive differentiations of the flat outputs one can transform the state-space model of the system into the canonical Brunovsky form and design a stabilizing feedback controller about it using the eigenvalues assignment technique.

3.2 Design of A Flatness-Based Controller

To obtain the input-output linearized equivalent state-space description of the six-phase power generator, the flat outputs of the system are successively differentiated until the control inputs reappear. By differentiating the first row of the state-space model of Eq. (47) one has

$$\ddot{x}_1 = \frac{1}{J}\mu\frac{L_m}{L_m + L_r}[(\dot{x}_4 + \dot{x}_6)x_2 + (x_4 + x_6)\dot{x}_2] - \dot{T_m} - b\dot{x}_1 \tag{48}$$

By considering that the wind induced torque T_m is piecewise constant and by substituting the derivatives $\dot{x}_1, \dot{x}_2, \dot{x}_4$ and $\dot{x}_6$ one obtains

$$\begin{aligned}\ddot{x}_1 = {} & \frac{1}{J}\mu\frac{L_m}{L_m + L_r}\left\{\frac{1}{L_{s_1}}\left[-R_{s_1}x_4 - \omega_s\left(L_{s_1}x_3 + x_2\right)\right]\right\}x_2 \\ & + \frac{1}{J}\mu\frac{L_m}{L_m + L_r}\left\{\frac{1}{L_{s_2}}\left[-R_{s_2}x_6 - \omega_s\left(L_{s_2}\right)x_5 + x_2\right]\right\}x_2 \\ & + \frac{1}{J}\mu\frac{L_m}{L_m + L_r}(x_4 + x_6)\left[-\frac{R_r}{L_m + L_r}x_2 + \frac{R_rL_r}{L_m + L_r}(x_3 + x_5)\right] \\ & - \frac{b}{J}\frac{1}{J}\left[\mu\frac{L_m}{L_m + L_r}(x_4 + x_6)x_2 - T_m - bx_1\right] \\ & + \left[\frac{1}{J}\mu\frac{L_m}{L_m + L_r}\left(-\frac{\omega_s}{L_{s_1}}x_2\right)\right]u_2 + \left[\frac{1}{J}\mu\frac{L_m}{L_m + L_r}\left(-\frac{\omega_s}{L_s}x_2\right)\right]u_4\end{aligned} \tag{49}$$

By grouping the terms that appear in the first three rows of Eq. (49) into the term $\bar{f}_1(x)$ as well as the terms that multiply u_2, u_4 into $\bar{g}_{21}(x)$ and $\bar{g}_{41}(x)$ respectively, (49) can be written in *a* concise form as

$$\ddot{x}_1 = \bar{f}_1(x) + \bar{g}_{21}(x)u_2 + \bar{g}_{41}(x)u_4 \tag{50}$$

Moreover, by differentiating the second row of the state-space model one has

$$\ddot{x}_2 = -\frac{R_r}{L_m + L_r}\dot{x}_2 + \frac{R_rL_m}{L_m + L_r}(\dot{x}_3 + \dot{x}_5) \tag{51}$$

By substituting the derivatives $\dot{x}_2, \dot{x}_3, \dot{x}_5$ and after intermediate operations one obtains

$$\begin{aligned}\ddot{x}_2 = {} & -\frac{R_r}{L_m + L_r}\left[-\frac{R_r}{L_m + L_r}x_2 + \frac{R_rL_m}{L_m + L_r}(x_3 + x_5)\right] \\ & + \frac{R_rL_m}{L_m + L_r}\frac{1}{L_{s_1}}\left[-R_{s1}x_3 + \omega_s\left(L_{s1}x_4 + \frac{L_mL_r}{L_m + L_r}(x_4 + x_6)\right)\right] \\ & + \frac{R_rL_m}{L_m + L_r}\frac{1}{L_{s_1}}\left[-R_{s2}x_5 + \omega_s\left(L_{s2}x_6 + \frac{L_mL_r}{L_m + L_r}(x_4 + x_6)\right)\right] \\ & + \left[\frac{R_rL_m}{L_m + L_r}\frac{1}{L_{s1}}\frac{\omega_s}{L_{s1}}\right]u_1 + \left[\frac{R_rL_m}{L_m + L_r}\frac{1}{L_{s2}}\frac{\omega_s}{L_{s2}}\right]u_3\end{aligned} \tag{52}$$

By grouping the terms that appear in the first three rows of Eq. (52) into the term $\bar{f}_2(x)$ as well as the terms that multiply u_1, u_3 into $\bar{g}_{12}(x)$ and $\bar{g}_{32}(x)$ respectively, (49) can be written in *a* concise form as

$$\ddot{x}_2 = \bar{f}_2(x) + \bar{g}_{12}(x)u_2 + \bar{g}_{32}(x)u_3 \tag{53}$$

Using Eq. (50) and Eq. (53), as well as the third and fourth rows of the state-space model of Eq. (47), the input-output linearized description of the dynamics of the six-phase induction generator is obtained

$$\begin{aligned}\ddot{x}_1 &= \bar{f}_1(x) + \bar{g}_{21}(x)u_2 + \bar{g}_{41}(x)u_4\\ \ddot{x}_2 &= \bar{f}_2(x) + \bar{g}_{12}(x)u_1 + \bar{g}_{32}(x)u_3\\ \dot{x}_3 &= f_3(x) + g_{13}(x)u_1\\ \dot{x}_4 &= f_4(x) + g_{24}(x)u_2\end{aligned} \tag{54}$$

Next, the state vector of the system is redefined as

$$z = [z_1, z_2, z_3, z_4, z_5, z_6]^T \Rightarrow z = [x_1, \dot{x}_1, x_2, \dot{x}_2, x_3, x_4]^T \tag{55}$$

the dynamic model of the six-phase induction generator is written as

$$\begin{aligned}\dot{z}_1 &= z_2\\ \dot{z}_2 &= \bar{f}_1(z) + \bar{g}_{21}(z)u_2 + \bar{g}_{41}(z)u_4\\ \dot{z}_3 &= z_4\\ \dot{z}_4 &= \bar{f}_2(z) + \bar{g}_{12}(z)u_1 + \bar{g}_{32}(z)u_3\\ \dot{z}_5 &= f_3(z) + g_{13}(z)u_1\\ \dot{z}_6 &= f_4(z) + g_{24}(z)u_2\end{aligned} \tag{56}$$

Moreover, by defining the control inputs $v_1 = \bar{f}_1(z) + \bar{g}_{21}(z)u_2 + \bar{g}_{41}(z)u_4$, $v_2 = \bar{f}_2(z) + \bar{g}_{12}(z)u_1 + \bar{g}_{32}(z)u_3$, $v_3 = u_1$ and $v_4 = u_2$ one obtains an equivalent description of the system's dynamics in the canonical Brunovsky form, that is

$$\begin{pmatrix}\dot{z}_1\\ \dot{z}_2\\ \dot{z}_3\\ \dot{z}_4\\ \dot{z}_5\\ \dot{z}_6\end{pmatrix} = \begin{pmatrix}0&1&0&0&0&0\\ 0&0&0&0&0&0\\ 0&0&0&1&0&0\\ 0&0&0&0&0&0\\ 0&0&0&0&0&0\\ 0&0&0&0&0&0\end{pmatrix}\begin{pmatrix}z_1\\ z_2\\ z_3\\ z_4\\ z_5\\ z_6\end{pmatrix} + \begin{pmatrix}0&0&0&0\\ 1&0&0&0\\ 0&0&0&0\\ 0&1&0&0\\ 0&0&1&0\\ 0&0&0&1\end{pmatrix}\begin{pmatrix}u_1\\ u_2\\ u_3\\ u_4\end{pmatrix} \tag{57}$$

In concise form the input-output linearized dynamics of the six-phase induction generator and the associated stabilizing feedback control is written as

$$\begin{aligned}\ddot{z}_1 &= v_1 \quad & v_1 &= \ddot{z}_1^d - k_{11}\left(\dot{z}_1 - \dot{z}_1^d\right) - k_{21}\left(z_1 - z_1^d\right)\\ \ddot{z}_3 &= v_2 \quad & v_2 &= \ddot{z}_3^d - k_{13}\left(\dot{z}_3 - \dot{z}_3^d\right) - k_{23}\left(z_3 - z_3^d\right)\\ \dot{z}_5 &= v_3 \quad & v_3 &= \dot{z}_5^d - k_{15}\left(z_5 - z_5^d\right)\\ \dot{z}_6 &= v_4 \quad & v_4 &= \dot{z}_6^d - k_{16}\left(z_6 - z_6^d\right)\end{aligned} \tag{58}$$

By defining the tracking error variables $e_1 = z_1 - z_1^d, e_3 = z_3 - z_3^d, e_5 = z_5 - z_5^d \; and \; e_7 = z_7 - z_7^d$ one obtains the tracking error dynamics of the closed-loop system

$$\begin{aligned}
&\left(\ddot{z}_1 - \ddot{z}_1^d\right) + k_{11}\left(\dot{z}_1 - \dot{z}_1^d\right) + k_{21}\left(z_1 - z_1^d\right) = 0 \Rightarrow \ddot{e}_1 + k_{11}\dot{e}_1 + k_{21}e_1 = 0 \\
&\left(\ddot{z}_3 - \ddot{z}_3^d\right) + k_{13}\left(\dot{z}_3 - \dot{z}_3^d\right) + k_{23}\left(z_3 - z_3^d\right) = 0 \Rightarrow \ddot{e}_3 + k_{13}\dot{e}_3 + k_{23}e_3 = 0 \\
&\left(\dot{z}_5 - \dot{z}_5^d\right) + k_{15}\left(z_5 - z_5^d\right) = 0 \Rightarrow \dot{e}_5 + k_{15}e_5 = 0 \\
&\left(\dot{z}_6 - \dot{z}_6^d\right) + k_{16}\left(z_6 - z_6^d\right) = 0 \Rightarrow \dot{e}_6 + k_{15}e_6 = 0
\end{aligned} \tag{59}$$

and by selecting coefficients $(k_{11}, k_{21}), (k_{13}, k_{23}), k_{15}\ and\ k_{25}$ such that the associated characteristic polynomials to be Hurwitz stable one has

$$\begin{aligned}
&\lim_{t\to\infty} e_1(t) = 0 \Rightarrow \lim_{t\to\infty} z_1(t) = z_1^d(t) \Rightarrow \lim_{t\to\infty} x_1(t) = x_1^d(t) \\
&\lim_{t\to\infty} e_3(t) = 0 \Rightarrow \lim_{t\to\infty} z_3(t) = z_3^d(t) \Rightarrow \lim_{t\to\infty} x_2(t) = x_2^d(t) \\
&\lim_{t\to\infty} e_5(t) = 0 \Rightarrow \lim_{t\to\infty} z_5(t) = z_5^d(t) \Rightarrow \lim_{t\to\infty} x_3(t) = x_3^d(t) \\
&\lim_{t\to\infty} e_6(t) = 0 \Rightarrow \lim_{t\to\infty} z_6(t) = z_6^d(t) \Rightarrow \lim_{t\to\infty} x_4(t) = x_4^d(t)
\end{aligned} \tag{60}$$

Therefore, all flat outputs of the system converge to their setpoints. Besides, state variables x_5, x_6 being differential functions of the flat outputs converge also to their reference values. To compute the control inputs that should be applied to the initial nonlinear dynamics of the six-phase induction generator one uses that

$$\begin{pmatrix} v_1 \\ v_2 \\ v_3 \\ v_4 \end{pmatrix} = \begin{pmatrix} \bar{f}_1(z) \\ \bar{f}_2(z) \\ \bar{f}_3(z) \\ \bar{f}_4(z) \end{pmatrix} + \begin{pmatrix} 0 & \bar{g}_{21}(z) & 0 & \bar{g}_{41}(z) \\ \bar{g}_{12}(z) & 0 & \bar{g}_{32}(z) & 0 \\ g_{13}(z) & 0 & 0 & 0 \\ 0 & g_{24}(z) & 0 & 0 \end{pmatrix} \begin{pmatrix} u_1 \\ u_2 \\ u_3 \\ u_4 \end{pmatrix} \tag{61}$$

which after being written in concise form gives

$$v = F(z) + G(z)u \Rightarrow u = G(z)^{-1}[v - F(z)] \tag{62}$$

4. Approximate Linearization of the Dynamic Model of the 6-Phase DSIG

The dynamic model of the 6-phase DSIG undergoes approximate linearization around the temporary operating point (x^*, u^*) which is updated at each iteration of the control algorithm. Thus, the nonlinear state-space model of the DSIG, being initially in the form $\dot{x} = f(x) + g(x)u$ is now transformed into the equivalent linearized state-space form.

$$\dot{x} = Ax + Bu + \tilde{d} \tag{63}$$

The linearization point (x^*, u^*) is defined at each sampling instance by the present value of the system's state vector x^* and by the last sampled value of the control inputs vector u^*. The linearization process makes use of first-order Taylor series expansion and of the computation of the associated Jacobian matrices.

$$A = \nabla_x[f(x) + g(x)u]\ |_{(x^*,u^*)} \Rightarrow A = \nabla_x f(x)\ |_{(x^*,u^*)} \tag{64}$$

$$B = \nabla_u[f(x) + g(x)u]\ |_{(x^*,u^*)} \Rightarrow B = g(x)\ |_{(x^*,u^*)} \tag{65}$$

The term $\tilde{d}$ is the cumulative disturbances variable which may consist of (i) modeling errors due to the truncation of higher-order terms from the Taylor series expansion, (ii) exogenous perturbations (iii) sensor measurement noise of any distribution.

This linearization approach for implementing the nonlinear optimal control scheme results in an accurate system dynamics model. Consider for instance the following affine-in-the-input state-space model.

$$\begin{aligned}
&\dot{x} = f(x) + g(x)u \Rightarrow \\
&\dot{x} = [f(x^*) + \nabla_x f(x)\,|_{x^*}\,(x - x^*)] + [g(x^*) + \nabla_x g(x)\,|_{x^*}\,(x - x^*)]u^* + g(x^*)u^* + g(x^*)(u - u^*) + \tilde{d}_1 \Rightarrow \\
&\dot{x} = [\nabla_x f(x)\,|_{x^*} + \nabla_x g(x)\,|_{x^*}\,u^*]x + g(x^*)u - [\nabla_x f(x)\,|_{x^*} + \nabla_x g(x)\,|_{x^*}\,u^*]x^* + f(x^*) + g(x^*)u^* + \tilde{d}_1
\end{aligned} \tag{66}$$

where $\tilde{d}_1$ is the modelling error due to truncation of higher order terms in the Taylor series expansion of $f(x)$ and $g(x)$. Next, by defining $A = [\nabla_x f(x)\,|_{x^*} + \nabla_x g(x)\,|_{x^*}\,u^*]$, $B = g(x^*)$ one obtains.

$$\dot{x} = Ax + Bu - Ax^* + f(x^*) + g(x^*)u^* + \tilde{d}_1 \tag{67}$$

Moreover by denoting $\tilde{d} = -Ax^* + f(x^*) + g(x^*)u^* + \tilde{d}_1$ about the cumulative modelling error term in the Taylor series expansion procedure one has

$$\dot{x} = Ax + Bu + \tilde{d} \tag{68}$$

which is the approximately linearized model of the dynamics of the system of Eq. (63). The term $f(x^*)$ + $g(x^*)u^*$ is the derivative of the state vector at (x^*, u^*) which is almost annihilated by $-Ax^*$.

The computation of the Jacobian matrix $A = \nabla_x f(x)\,|_{(x^*,u^*)}$ proceeds as follows:

First row of the Jacobian matrix $A = \nabla_x f(x)\,|_{(x^*,u^*)}$: $\frac{\partial f_1}{\partial x_1} = -\frac{b}{J}, \frac{\partial f_1}{\partial x_2} = \frac{p}{J}\frac{L_m}{L_m+L_r}(x_4 + x_6), \frac{\partial f_1}{\partial x_3} = 0, \frac{\partial f_1}{\partial x_4} = \frac{p}{J}\frac{L_m}{L_m+L_r}x_2, \frac{\partial f_1}{\partial x_5} = 0$ *and* $\frac{\partial f_1}{\partial x_6} = \frac{p}{J}\frac{L_m}{L_m+L_r}x_2$.

Second row of the Jacobian matrix $A = \nabla_x f(x)\,|_{(x^*,u^*)}$: $\frac{\partial f_2}{\partial x_1} = 0, \frac{\partial f_2}{\partial x_2} = -\frac{R_r}{L_m+L_r}, \frac{\partial f_2}{\partial x_3} = \frac{R_r L_m}{L_m+L_r}, \frac{\partial f_2}{\partial x_4} = 0, \frac{\partial f_2}{\partial x_5} = \frac{R_r L_m}{L_m+L_r}$ *and* $\frac{\partial f_2}{\partial x_6} = 0$.

Third row of the Jacobian matrix $A = \nabla_x f(x)\,|_{(x^*,u^*)}$: $\frac{\partial f_3}{\partial x_1} = 0, \frac{\partial f_3}{\partial x_2} = 0, \frac{\partial f_3}{\partial x_3} = \frac{R_{s1}}{L_{s1}}, \frac{\partial f_3}{\partial x_4} = \frac{\omega_s}{L_{s1}}\left(L_{s_1} + \frac{L_m L_r}{L_m+L_r}\right), \frac{\partial f_3}{\partial x_5} = 0$ *and* $\frac{\partial f_3}{\partial x_6} = \frac{\omega_s}{L_{s1}}\frac{L_m L_r}{L_m+L_r}$.

Fourth row of the Jacobian matrix, $A = \nabla_x f(x)\,|_{(x^*,u^*)}$: $\frac{\partial f_4}{\partial x_1} = 0, \frac{\partial f_4}{\partial x_2} = -\frac{\omega_s}{L_{s1}}, \frac{\partial f_4}{\partial x_3} = -\omega_s, \frac{\partial f_4}{\partial x_4} = -\frac{R_{s1}}{L_{s1}}, \frac{\partial f_4}{\partial x_5} = 0$ *and* $\frac{\partial f_4}{\partial x_6} = 0$.

Fifth row of the Jacobian matrix, $A = \nabla_x f(x)\,|_{(x^*,u^*)}$: $\frac{\partial f_5}{\partial x_1} = 0, \frac{\partial f_5}{\partial x_2} = 0, \frac{\partial f_5}{\partial x_3} = 0, \frac{\partial f_5}{\partial x_4} = \frac{\omega_s}{L_{s2}}\frac{L_m L_r}{L_m+L_r}, \frac{\partial f_5}{\partial x_5} = -\frac{R_{s2}}{L_{s2}}$ *and* $\frac{\partial f_5}{\partial x_6} = \frac{\omega_s}{L_{s2}}(L_{s2} + \frac{L_m L_r}{L_m+L_r})$.

Sixth row of the Jacobian matrix $A = \nabla_x f(x)\,|_{(x^*,u^*)}$: $\frac{\partial f_6}{\partial x_1} = 0, \frac{\partial f_6}{\partial x_2} = -\frac{\omega_s}{L_{s2}}, \frac{\partial f_6}{\partial x_3} = 0, \frac{\partial f_6}{\partial x_4} = 0, \frac{\partial f_6}{\partial x_5} = -\omega_s$ *and* $\frac{\partial f_6}{\partial x_6} = -\frac{R_{s2}}{L_{s2}}$.

5. The Nonlinear H-Infinity Control

5.1 Min-Max Control and Disturbance Rejection

In the H_∞ control approach, a feedback control scheme is designed for setpoint tracking by the system's state vector and simultaneous disturbance rejection, considering that the disturbance affects the system in the worst possible manner. For the approximately linearized model of Eq. (63), the disturbances' effects are incorporated in the following quadratic cost function [40].

$$J(t) = \frac{1}{2}\int_0^T \left[y^T(t)y(t) + ru^T(t)u(t) - \rho^2\tilde{d}^T(t)\tilde{d}(t)\right]dt\,,\ r,\rho > 0 \tag{69}$$

The significance of the negative sign in the cost function's term that is associated with the perturbation variable $\tilde{d}(t)$ is that the disturbance tries to maximize the cost function $J(t)$ while the control signal $u(t)$ tries to minimize it.

The physical meaning of the above mentioned relation is that the control signal and the disturbances compete within a min-max differential game. This min-max optimization problem can be written as $min_u max_{\tilde{d}} J(u,\tilde{d})$. The objective of the optimization procedure is to compute a control signal $u(t)$ which can compensate for the worst possible disturbance that affects the system. However, the solution to the min-max optimization problem is directly related to the value of parameter ρ. This means that there is an upper bound in the disturbances magnitude that the control signal can tolerate.

5.2 Design of the Stabilizing Feedback Controller

After linearization around its current operating point (x^*, u^*), the dynamic model of the 6-phase dual-star induction generator is written as

$$\dot{x} = Ax + Bu + d_1 \tag{70}$$

Parameter d_1 stands for the linearization error in the 6-phase induction generator's model appearing previously in Eq. (70). The reference setpoints for the state vector of the six-phase induction generator are denoted by $x_d = [x_1^d, \cdots, x_6^d]$. Tracking of this trajectory is achieved after applying the control input u_d. At every time instant the control input u_d is assumed to differ from the control input u appearing in Eq. (70) by an amount equal to Δu, that is $u_d = u + \Delta u$.

$$\dot{x}_d = Ax_d + Bu_d + d_2 \tag{71}$$

The dynamics of the controlled system described in Eq. (70) can be also written as

$$\dot{x} = Ax + Bu + Bu_d - Bu_d + d_1 \tag{72}$$

and by denoting $d_3 = -Bu_d + d_1$ as an aggregate disturbance term one obtains

$$\dot{x} = Ax + Bu + Bu_d + d_3 \tag{73}$$

By subtracting Eq. (71) from Eq. (73) one has

$$\dot{x} - \dot{x}_d = A(x - x_d) + Bu + d_3 - d_2 \tag{74}$$

By denoting the tracking error as $e = x - x_d$ and the aggregate disturbance term as $\tilde{d} = d_3 - d_2$, the tracking error dynamics becomes

$$\dot{e} = Ae + Bu + \tilde{d} \tag{75}$$

For the linearized system the cost function of Eq. (69) is defined, where coefficient *r* determines the penalization of the control input and the weight coefficient *ρ* determines the reward of the disturbances' effects. Then, the optimal feedback control law is given by

$$u(t) = -Kx(t) \tag{76}$$

with $K = \frac{1}{r}B^T P$ where *P* is a positive definite symmetric matrix which is obtained from the solution of the Riccati equation.

$$A^T P + PA + Q - P\left(\frac{2}{r}BB^T - \frac{1}{\rho^2}LL^T\right)P = 0 \tag{77}$$

where *Q* is also a semi-positive definite symmetric matrix.The worst-case disturbance is given by $\tilde{d}(t) = \frac{1}{\rho^2}L^T P x(t)$. The computation of the worst-case disturbance that this controller can sustain, comes from the superposition of Bellman's optimality principle when considering that the six-phase induction generator is affected by two separate inputs, the control input *u* and the cumulative disturbance input $\tilde{d}$. From the previous relation about the worst-case disturbance, it can be seen that the smallest value of the attenuation coefficient *ρ* that results in an admissible solution for the method's algebraic Riccati equation, is the one that provides the control loop with maximum robustness. The diagram of the considered control loop is depicted in Figure 3.

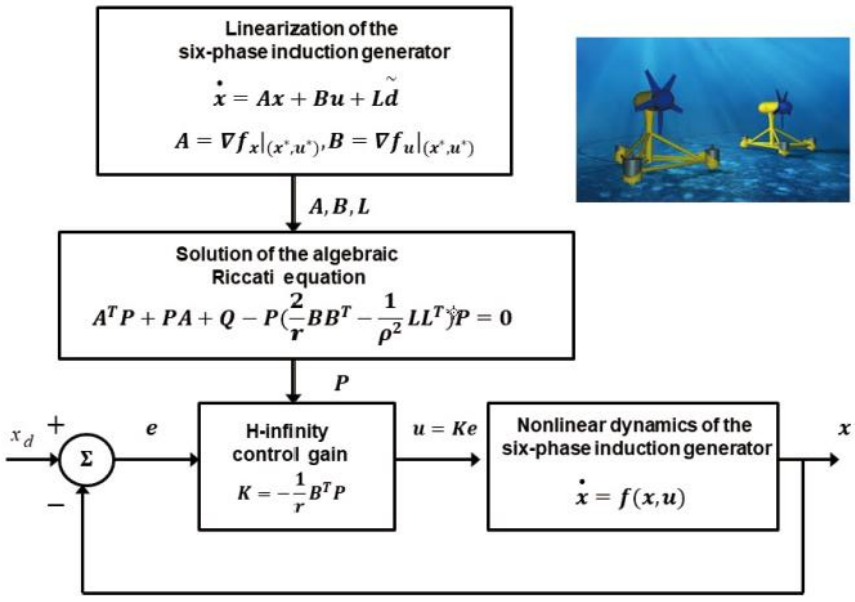

Figure 3 Diagram of the Nonlinear Optimal Control loop for a 6-phase dual star induction generator (with potential for using in a marine-turbine power generation unit).

6. Lyapunov Stability Analysis

6.1 Stability Proof

Through Lyapunov stability analysis it will be shown that the proposed nonlinear control scheme assures H_∞ tracking performance for the 6-phase induction generator, and that in case of bounded disturbance terms asymptotic convergence to the reference setpoints is achieved. The tracking error dynamics for the 6-phase induction generator are written in the form [40].

$$\dot{e} = Ae + Bu + L\tilde{d} \tag{78}$$

In the 6-phase induction generator's case $L \in R^{6\times 6}$ is the disturbance inputs gain matrix. Variable $\tilde{d}$ denotes model uncertainties and external disturbances of the generator's model. The following Lyapunov equation is considered.

$$V = \frac{1}{2}e^T Pe \tag{79}$$

where $e = x - x_d$ is the tracking error. By differentiating with respect to time one obtains.

$$\dot{V} = \frac{1}{2}\dot{e}^T Pe + \frac{1}{2}e^T P\dot{e} \Rightarrow \dot{V} = \frac{1}{2}\left[Ae + Bu + L\tilde{d}\right]^T Pe + \frac{1}{2}e^T P\left[Ae + Bu + L\tilde{d}\right] \Rightarrow \tag{80}$$

$$\dot{V} = \frac{1}{2}\left[e^T A^T + u^T B^T + \tilde{d}^T L^T\right]Pe + \frac{1}{2}e^T P\left[Ae + Bu + L\tilde{d}\right] \Rightarrow \tag{81}$$

$$\dot{V} = \frac{1}{2}e^T A^T Pe + \frac{1}{2}u^T B^T Pe + \frac{1}{2}\tilde{d}^T L^T Pe + \frac{1}{2}e^T PAe + \frac{1}{2}e^T PBu + \frac{1}{2}e^T PL\tilde{d} \tag{82}$$

The previous equation is rewritten as

$$\dot{V} = \frac{1}{2}e^T(A^T P + PA)e + \left(\frac{1}{2}u^T B^T Pe + \frac{1}{2}e^T PBu\right) + \left(\frac{1}{2}\tilde{d}^T L^T Pe + \frac{1}{2}e^T PL\tilde{d}\right) \tag{83}$$

Assumption: For given positive definite matrix Q and coefficients r and ρ there exists a positive definite matrix P, which is the solution of the following matrix equation.

$$A^T P + PA = -Q + P\left(\frac{2}{r}BB^T - \frac{1}{\rho^2}LL^T\right)P \tag{84}$$

Moreover, the following feedback control law is applied to the system.

$$u = -\frac{1}{r}B^T Pe \tag{85}$$

By substituting Eq. (84) and Eq. (85) one obtains.

$$\dot{V} = \frac{1}{2}e^T\left[-Q + P\left(\frac{2}{r}BB^T - \frac{1}{\rho^2}LL^T\right)P\right]e + e^T PB\left(-\frac{1}{r}B^T Pe\right) + e^T PL\tilde{d} \Rightarrow \tag{86}$$

$$\dot{V} = -\frac{1}{2}e^T Qe + \left(\frac{1}{r}e^T PBB^T Pe - \frac{1}{2\rho^2}e^T PLL^T Pe\right) - \frac{1}{r}e^T PBB^T Pe + e^T PL\tilde{d} \tag{87}$$

which after intermediate operations gives.

$$\dot{V} = -\frac{1}{2}e^T Qe - \frac{1}{2\rho^2}e^T PLL^T Pe + e^T PL\tilde{d} \tag{88}$$

or, equivalently

$$\dot{V} = -\frac{1}{2}e^T Qe - \frac{1}{2\rho^2}e^T PLL^T Pe + \frac{1}{2}e^T PL\tilde{d} + \frac{1}{2}\tilde{d}^T L^T Pe \tag{89}$$

Lemma: The following inequality holds [40].

$$\frac{1}{2}e^T L\tilde{d} + \frac{1}{2}\tilde{d}L^T Pe - \frac{1}{2\rho^2}e^T PLL^T Pe \leq \frac{1}{2}\rho^2\tilde{d}^T\tilde{d} \tag{90}$$

Proof: The binomial $(\rho\alpha - \frac{1}{\rho}b)^2$ is considered. Expanding the left part of the above inequality one gets.

$$\begin{aligned}&\rho^2 a^2 + \frac{1}{\rho^2}b^2 - 2ab \geq 0 \Rightarrow \frac{1}{2}\rho^2 a^2 + \frac{1}{2\rho^2}b^2 - ab \geq 0 \Rightarrow \\ &ab - \frac{1}{2\rho^2}b^2 \leq \frac{1}{2}\rho^2 a^2 \Rightarrow \frac{1}{2}ab + \frac{1}{2}ab - \frac{1}{2\rho^2}b^2 \leq \frac{1}{2}\rho^2 a^2\end{aligned} \tag{91}$$

The following substitutions are carried out $a = \tilde{d}$ and $b = e^T PL$ and the previous relation becomes.

$$\frac{1}{2}\tilde{d}^T L^T Pe + \frac{1}{2}e^T PL\tilde{d} - \frac{1}{2\rho^2}e^T PLL^T Pe \leq \frac{1}{2}\rho^2\tilde{d}^T\tilde{d} \tag{92}$$

Eq. (92) is substituted in Eq. (89) and the inequality is enforced, thus giving [40].

$$\dot{V} \leq -\frac{1}{2}e^T Qe + \frac{1}{2}\rho^2\tilde{d}^T\tilde{d} \tag{93}$$

Eq. (93) shows that the H_∞ tracking performance criterion is satisfied. The integration of $\dot{V}$ from 0 to *T* gives.

$$\begin{aligned}&\int_0^T \dot{V}(t)dt \leq -\frac{1}{2}\int_0^T ||e||_Q^2 dt + \frac{1}{2}\rho^2\int_0^T ||\tilde{d}||^2 dt \Rightarrow \\ &2V(T) + \int_0^T ||e||_Q^2 dt \leq 2V(0) + \rho^2\int_0^T ||\tilde{d}||^2 dt\end{aligned} \tag{94}$$

Moreover, if there exists a positive constant $M_d > 0$ such that

$$\int_0^\infty ||\tilde{d}||^2\, dt \leq M_d \tag{95}$$

then one gets.

$$\int_0^\infty ||e||_Q^2 dt \leq 2V(0) + \rho^2 M_d \tag{96}$$

Thus, the integral $\int_0^\infty ||e||_Q^2 dt$ is bounded. Moreover, $V(T)$ is bounded and from the definition of the Lyapunov function V in Eq. (79) it becomes clear that $e(t)$ will also be bounded since $e(t) \in \Omega_e = \{e|e^T Pe \leq 2V(0) + \rho^2 M_d\}$. According to the above and with the use of Barbalat's Lemma one obtains $lim_{t\to\infty} e(t) = 0$.

After following the stages of the stability proof one arrives at Eq. (93) which shows that the H-infinity tracking performance criterion holds. By selecting the attenuation coefficient ρ to be sufficiently small and in particular to satisfy $\rho^2 < ||e||^2_Q / ||\tilde{d}||^2$ one has that the first derivative of the Lyapunov function is upper bounded by 0. This condition holds at each sampling instance and consequently global stability for the control loop can be concluded.

6.2 Robust State Estimation with the Use of the H_∞ Kalman Filter

The control loop has to be implemented using information provided by a few sensors and by processing only a small number of state variables. One can implement feedback control by measuring only the stator currents. To reconstruct the missing information about the state vector of the 6-phase induction generator it is proposed to use a filtering scheme and based on it apply state estimation-based control [40]. By denoting as $A(k)$, $B(k)$ and $C(k)$ the discrete-time equivalents of matrices A, B and C of the linearized state-space model of the system, the recursion of the H_∞ Kalman Filter, for the model of the 6-phase induction generator, can be formulated in terms of a *measurement update* and a *time update* part.

6.2.1 Measurement Update

$$\begin{aligned} D(k) &= [I - \theta W(k)P^-(k) + C^T(k)R(k)^{-1}C(k)P^-(k)]^{-1} \\ K(k) &= P^-(k)D(k)C^T(k)R(k)^{-1} \\ \hat{x}(k) &= \hat{x}^-(k) + K(k)[y(k) - C\hat{x}^-(k)] \end{aligned} \tag{97}$$

6.2.2 Time Update

$$\begin{aligned} \hat{x}^-(k+1) &= A(k)x(k) + B(k)u(k) \\ P^-(k+1) &= A(k)P^-(k)D(k)A^T(k) + Q(k) \end{aligned} \tag{98}$$

where it is assumed that parameter θ is sufficiently small to assure that the covariance matrix $P^-(k)^{-1} - \theta W(k) + C^T(k)R(k)^{-1}C(k)$ will be positive definite. When $\theta = 0$ the H_∞ Kalman Filter becomes equivalent to the standard Kalman Filter. One can measure only a part of the state vector of the six-phase induction generator, and can estimate through filtering the rest of the state vector elements. For instance, one can process measurements of state variables x_1 to x_4 and estimate by filtering the stator's second-frame currents x_5, x_6.

7. Simulation Tests

The fine performance of the nonlinear optimal control scheme for the dynamic model of the 6-phase induction generator is further confirmed through simulation experiments. The simulation code has been developed in Matlab and the repetitive solution of the control method's algebraic Riccati equation was performed at each sampling period using Matlab's function *resolve ()*. The functioning of the 6-phase induction generator was tested under various operating conditions associated with time-varying or abruptly changing setpoints for the system's state variables. The obtained results are depicted in Figure 4 to Figure 19. The real values of the state variables are depicted in blue, the associated setpoints are printed in red and the estimated values of the state vector elements are plotted in green. In all simulation tests, fast and accurate tracking of the reference setpoints by the state variables of the six-phase induction machine can be achieved under moderate variations of the control inputs. The method remains computationally efficient. The solution of the algebraic Riccati equation which is used for defining the gains of the H-infinity feedback controller is performed on a PC with an Intel i7 processor at 2.8 GHz within a time-interval much shorter than the sampling period T_s = 0.01sec of the control algorithm.

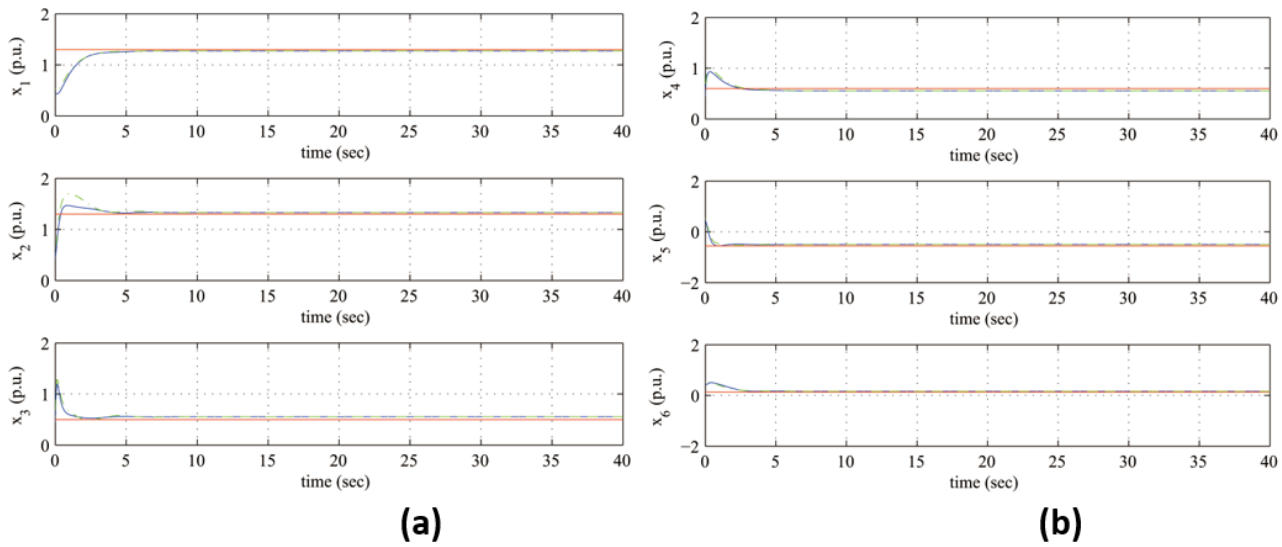

Figure 4 Tracking of setpoint 1 for the renewable energy system which is based on a six-phase induction generator (a) convergence of state variables x_1 to x_3 to their reference setpoints (red line: setpoint, blue line: real value, green line: estimated value), (b) convergence of state variables x_4 to x_6 to their reference setpoints (red line: setpoint, blue line: real value, green line: estimated value).

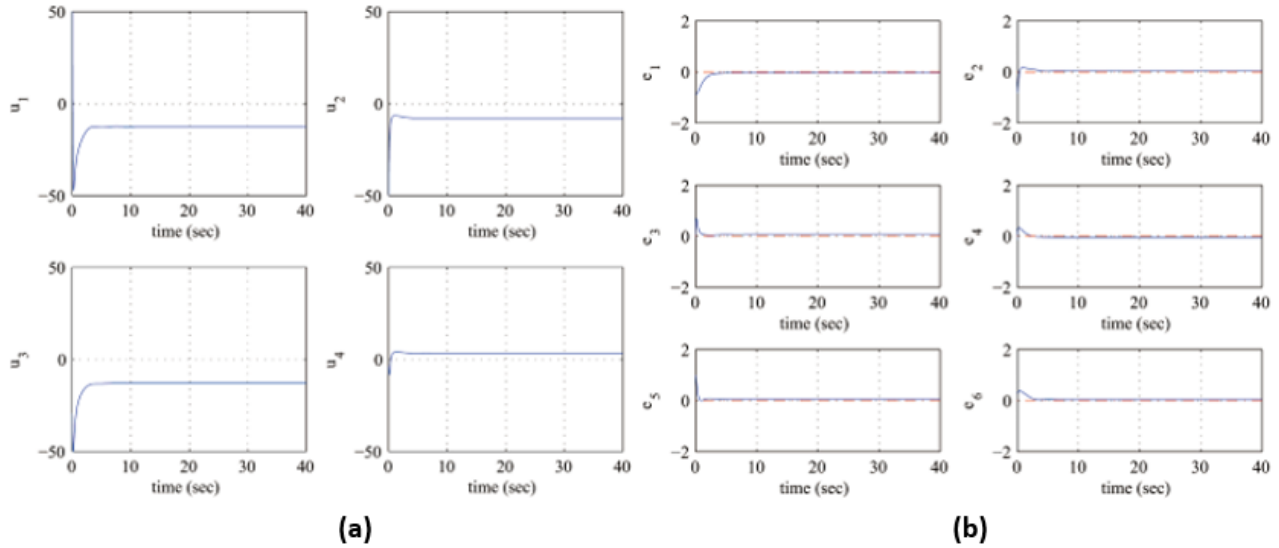

Figure 5 Tracking of setpoint 1 for the renewable energy system which is based on a six-phase induction generator (a) control inputs u_1 to u_4, (b) convergence to zero of the tracking error for the state variables of the six-phase induction generator.

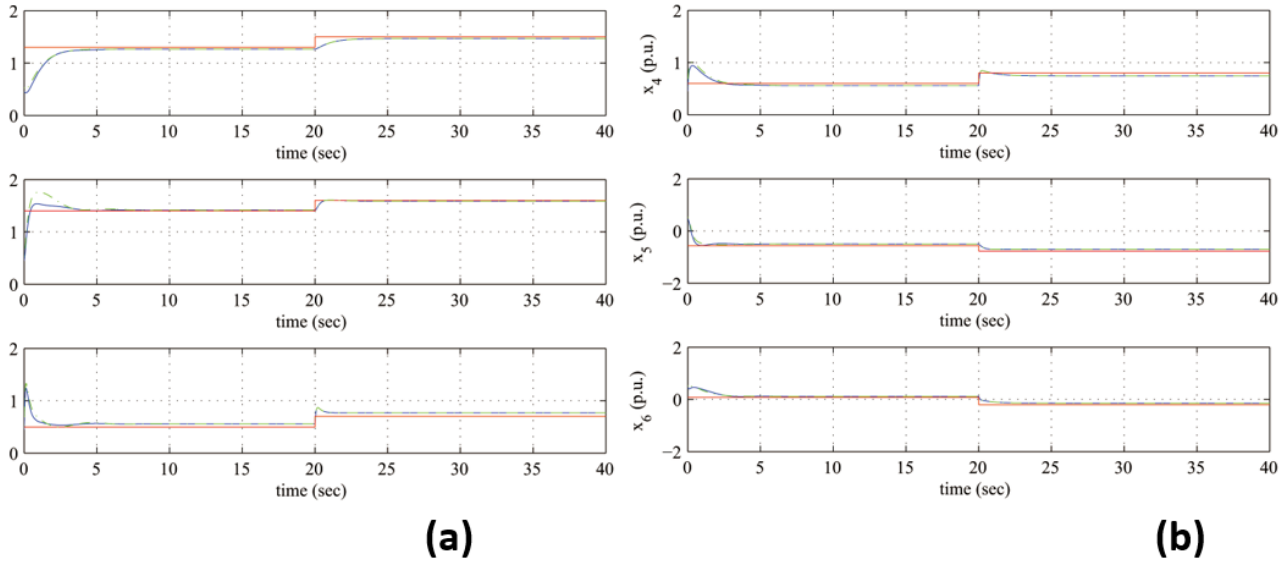

Figure 6 Tracking of setpoint 2 for the renewable energy system which is based on a six-phase induction generator (a) convergence of state variables x_1 to x_3 to their reference setpoints (red line: setpoint, blue line: real value, green line: estimated value), (b) convergence of state variables x_4 to x_6 to their reference setpoints (red line: setpoint, blue line: real value, green line: estimated value).

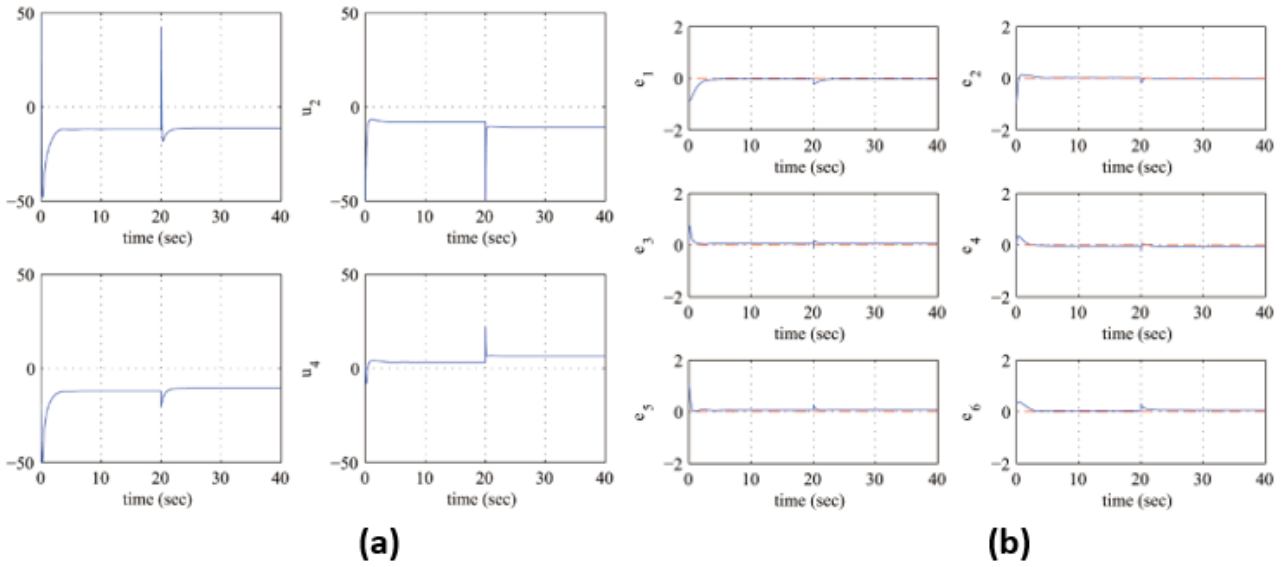

Figure 7 Tracking of setpoint 2 for the renewable energy system which is based on a six-phase induction generator (a) control inputs u_1 to u_4, (b) convergence to zero of the tracking error for the state variables of the six-phase induction generator.

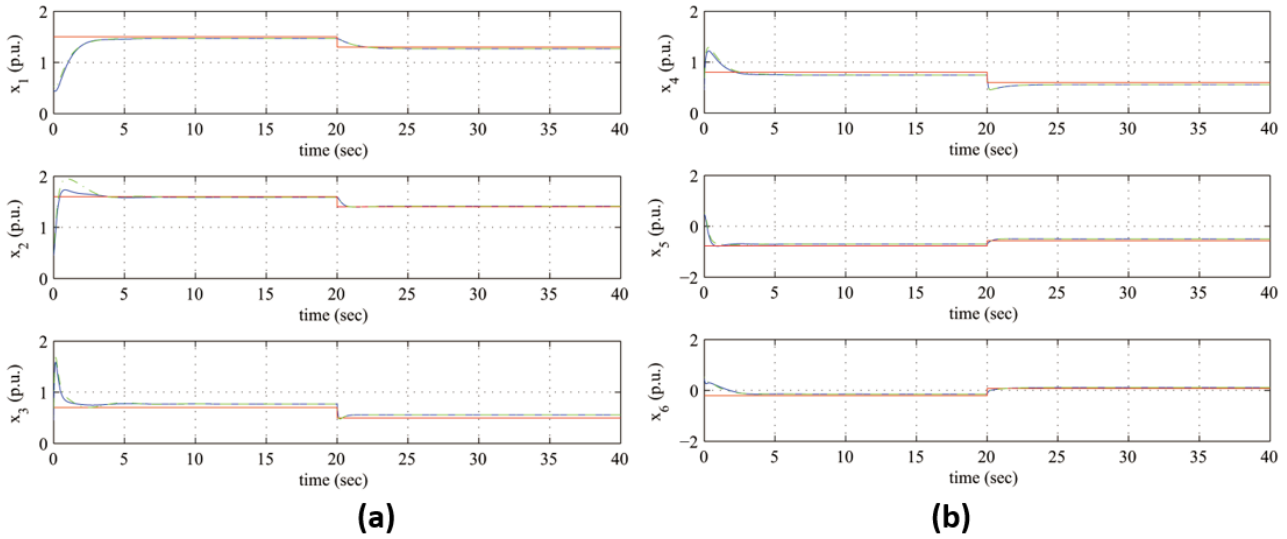

Figure 8 Tracking of setpoint 3 for the renewable energy system which is based on a six-phase induction generator (a) convergence of state variables x_1 to x_3 to their reference setpoints (red line: setpoint, blue line: real value, green line: estimated value), (b) convergence of state variables x_4 to x_6 to their reference setpoints (red line: setpoint, blue line: real value, green line: estimated value).

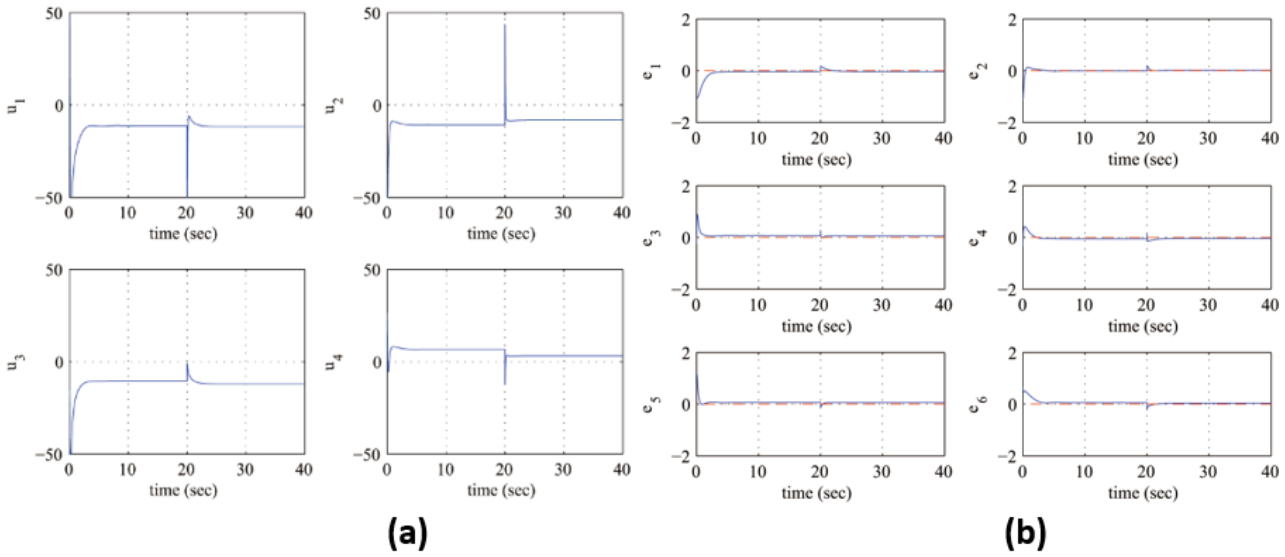

Figure 9 Tracking of setpoint 3 for the renewable energy system which is based on a six-phase induction generator (a) control inputs u_1 to u_4, (b) convergence to zero of the tracking error for the state variables of the six-phase induction generator.

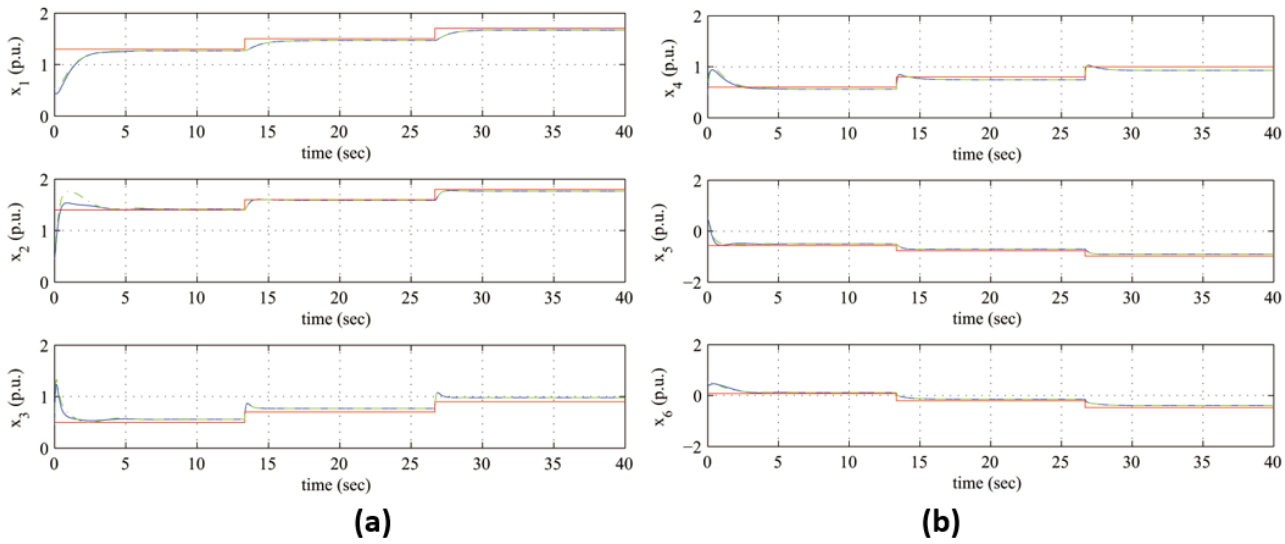

Figure 10 Tracking of setpoint 4 for the renewable energy system which is based on a six-phase induction generator (a) convergence of state variables x_1 to x_3 to their reference setpoints (red line: setpoint, blue line: real value, green line: estimated value), (b) convergence of state variables x_4 to x_6 to their reference setpoints (red line: setpoint, blue line: real value, green line: estimated value).

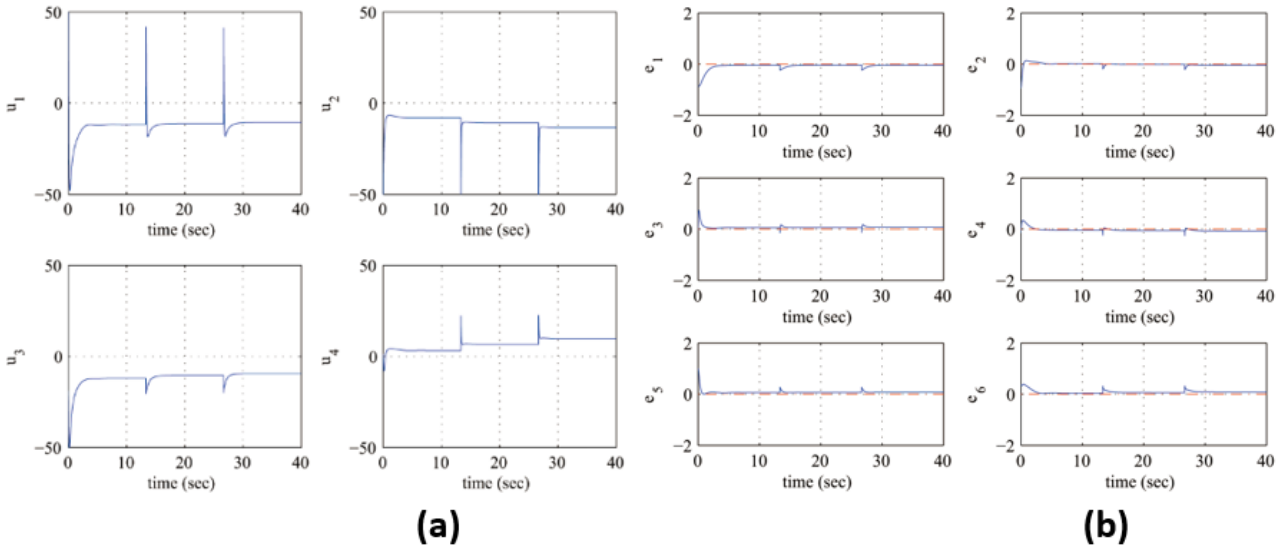

Figure 11 Tracking of setpoint 4 for the renewable energy system which is based on a six-phase induction generator (a) control inputs u_1 to u_4, (b) convergence to zero of the tracking error for the state variables of the six-phase induction generator.

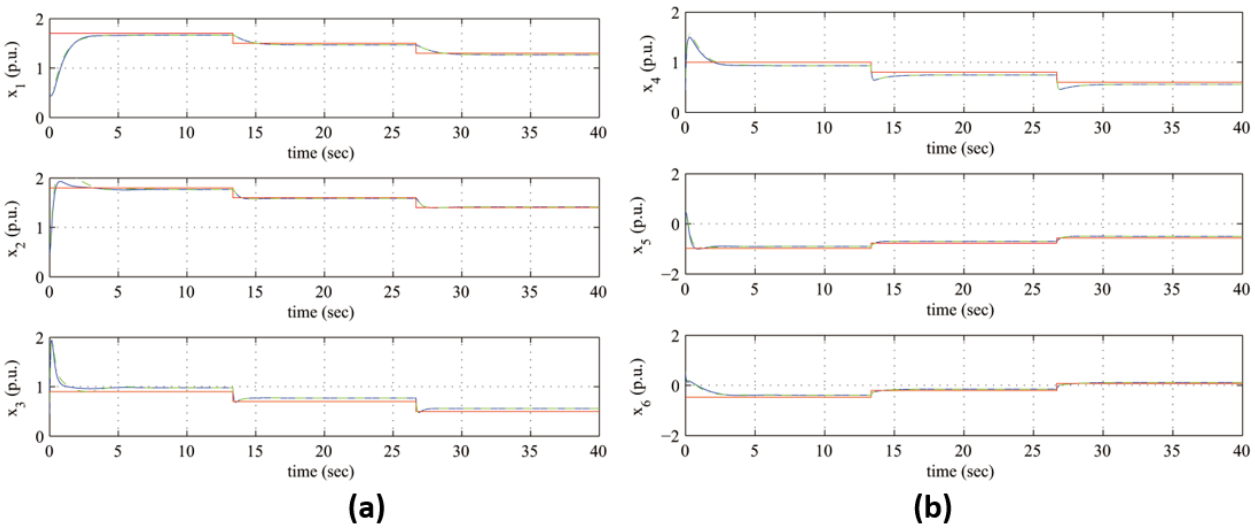

Figure 12 Tracking of setpoint 5 for the renewable energy system which is based on a six-phase induction generator (a) convergence of state variables x_1 to x_3 to their reference setpoints (red line: setpoint, blue line: real value, green line: estimated value), (b) convergence of state variables x_4 to x_6 to their reference setpoints (red line: setpoint, blue line: real value, green line: estimated value).

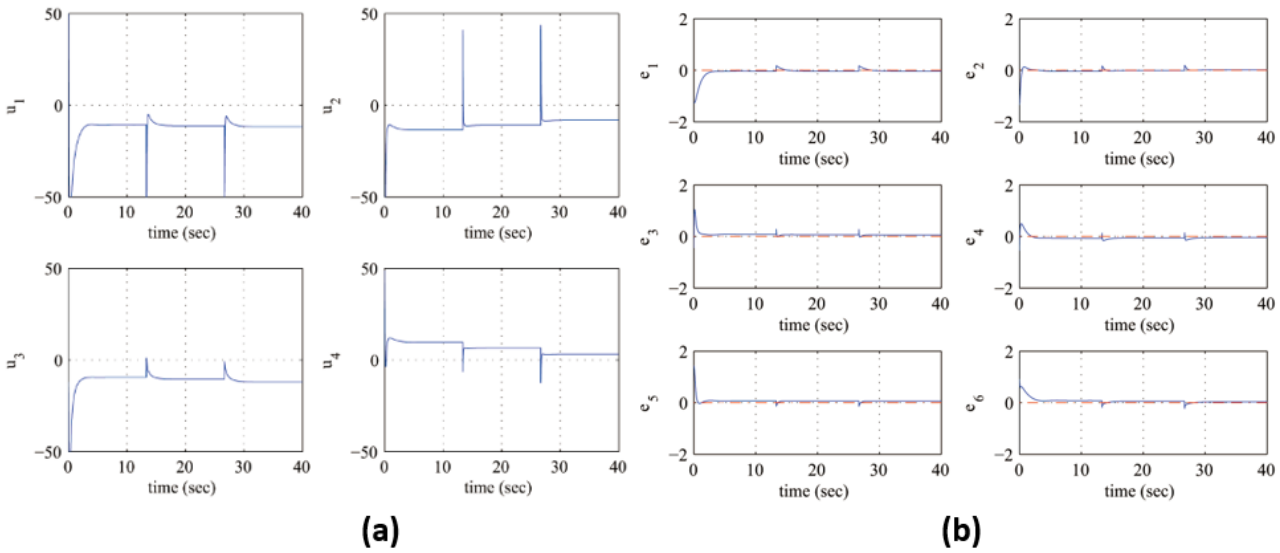

Figure 13 Tracking of setpoint 5 for the renewable energy system which is based on a six-phase induction generator (a) control inputs u_1 to u_4, (b) convergence to zero of the tracking error for the state variables of the six-phase induction generator.

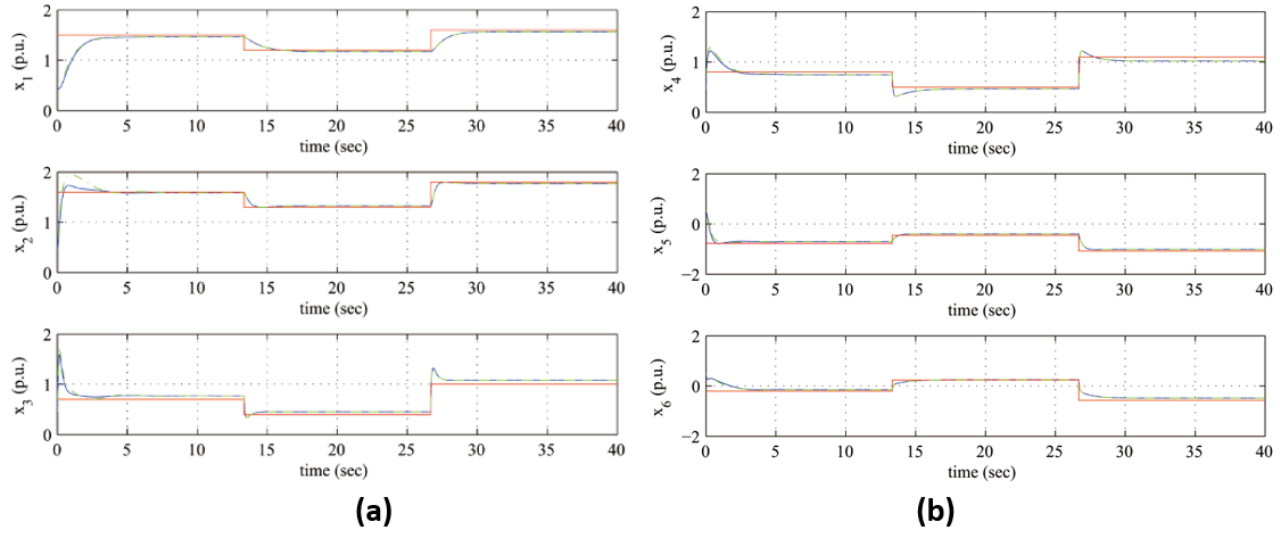

Figure 14 Tracking of setpoint 6 for the renewable energy system which is based on a six-phase induction generator (a) convergence of state variables x_1 to x_3 to their reference setpoints (red line: setpoint, blue line: real value, green line: estimated value), (b) convergence of state variables x_4 to x_6 to their reference setpoints (red line: setpoint, blue line: real value, green line: estimated value).

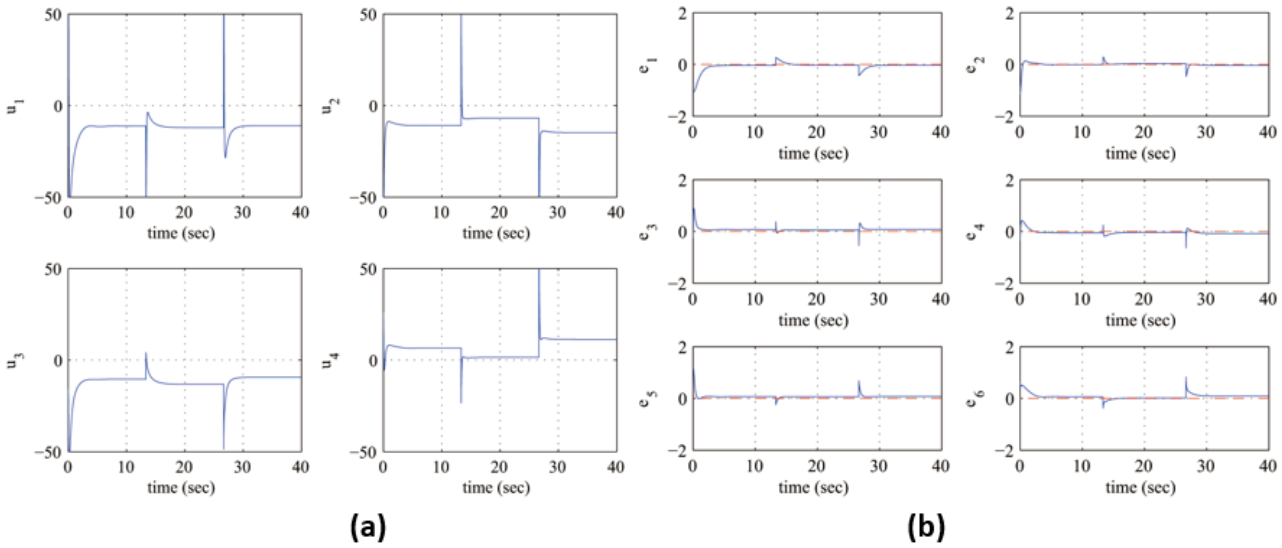

Figure 15 Tracking of setpoint 6 for the renewable energy system which is based on a six-phase induction generator (a) control inputs u_1 to u_4, (b) convergence to zero of the tracking error for the state variables of the six-phase induction generator.

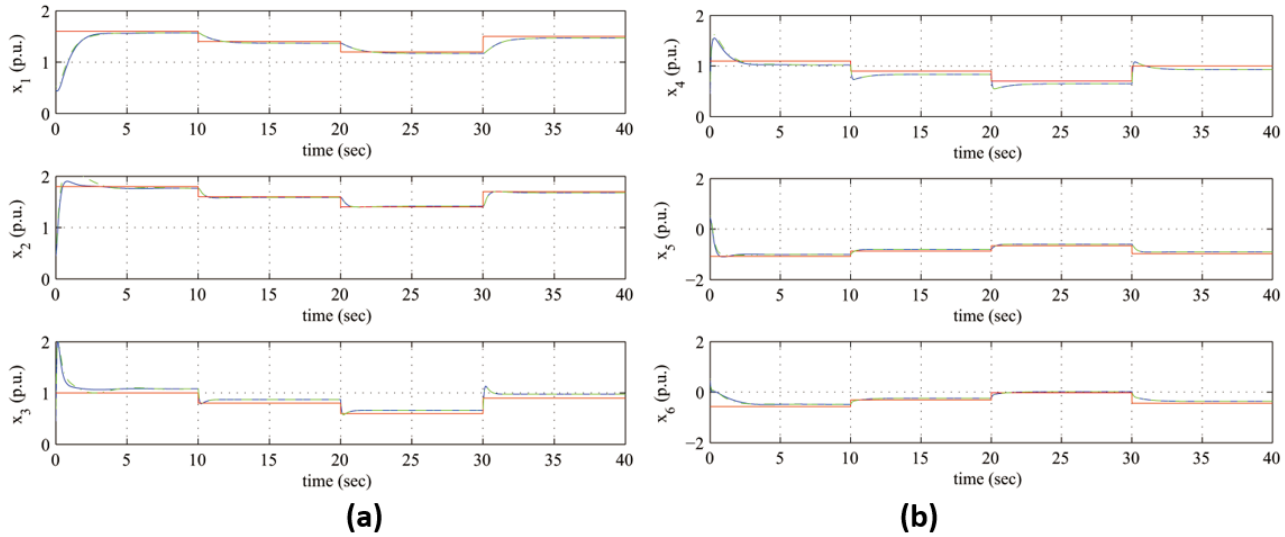

Figure 16 Tracking of setpoint 7 for the renewable energy system which is based on a six-phase induction generator (a) convergence of state variables x_1 to x_3 to their reference setpoints (red line: setpoint, blue line: real value, green line: estimated value), (b) convergence of state variables x_4 to x_6 to their reference setpoints (red line: setpoint, blue line: real value, green line: estimated value).

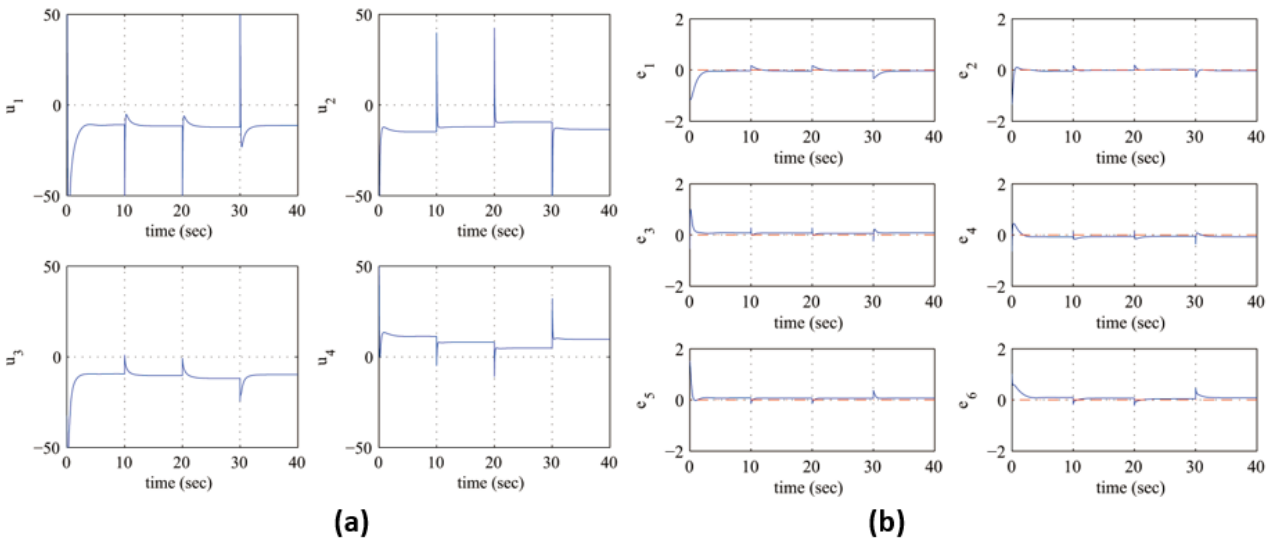

Figure 17 Tracking of setpoint 7 for the renewable energy system which is based on a six-phase induction generator (a) control inputs u_1 to u_4, (b) convergence to zero of the tracking error for the state variables of the six-phase induction generator.

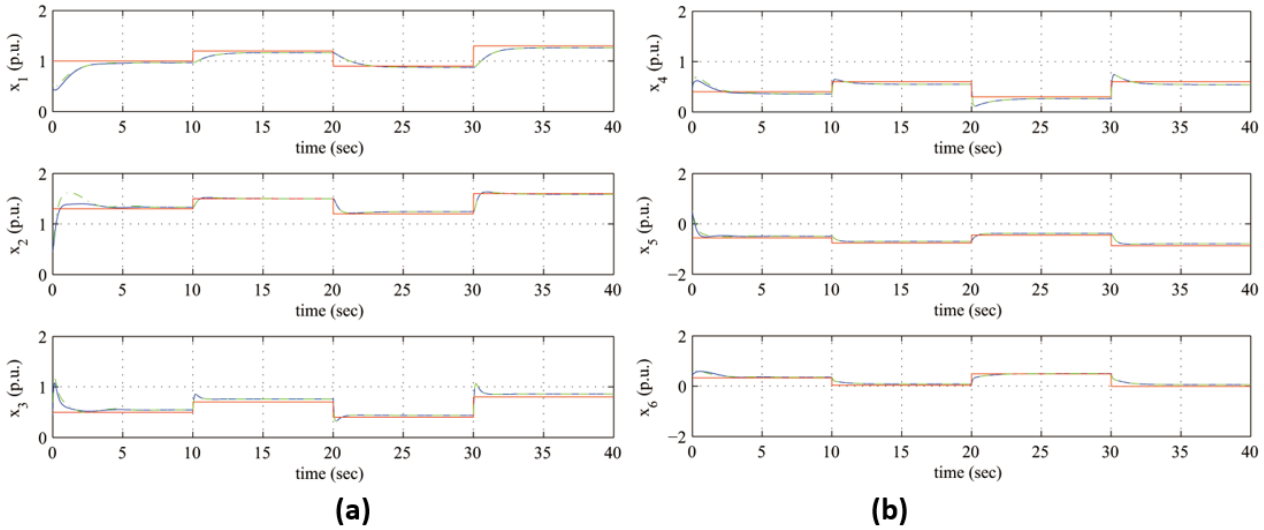

Figure 18 Tracking of setpoint 8 for the renewable energy system which is based on a six-phase induction generator (a) convergence of state variables x_1 to x_3 to their reference setpoints (red line: setpoint, blue line: real value, green line: estimated value), (b) convergence of state variables x_4 to x_6 to their reference setpoints (red line: setpoint, blue line: real value, green line: estimated value).

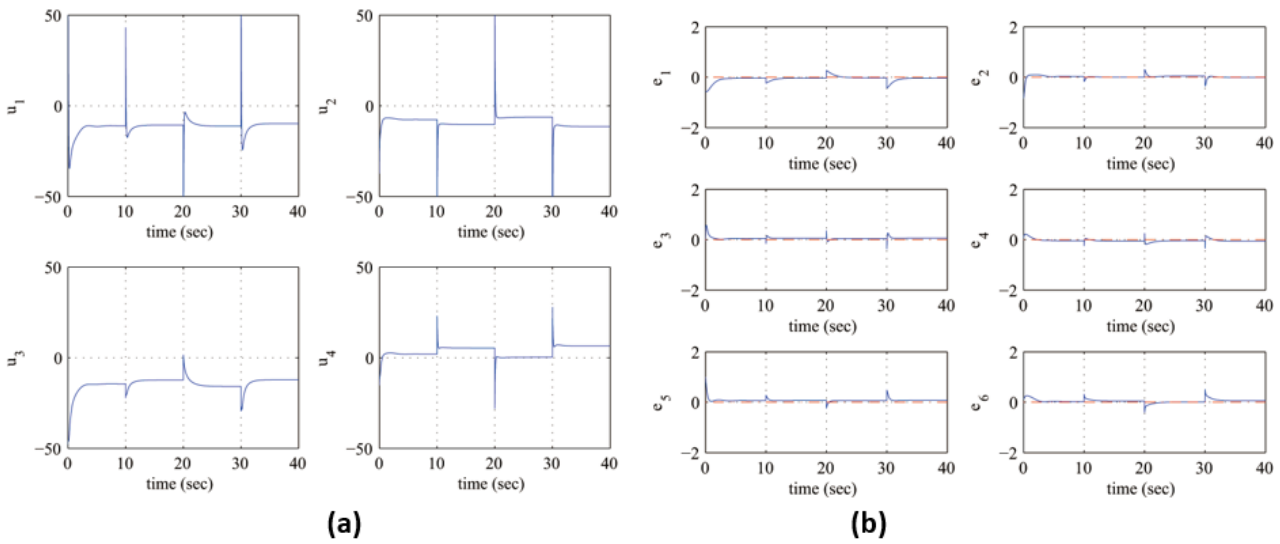

Figure 19 Tracking of setpoint 8 for the renewable energy system which is based on a six-phase induction generator (a) control inputs u_1 to u_4, (b) convergence to zero of the tracking error for the state variables of the six-phase induction generator.

To elaborate on the tracking performance and on the robustness of the proposed nonlinear optimal control method for the six-phase induction generator the following Tables are given: (i) Table 2 which provides information about the accuracy of tracking of the reference setpoints by the state variables of the six-phase induction generator's state-space model, (ii) Table 3 which provides information about the robustness of the control method to parametric changes in the model of the six-phase induction generator (change $\Delta a\%$ in resistance R_2 of the second three-phase frame of the stator), (iii) Table 4 which provides information about the precision in state variables' estimation that is achieved by the H-infinity Kalman Filter, (iv) Table 5 which provides the indicative convergence times of the six-phase induction generator's state variables to the associated setpoints.

Table 2 Tracking RMSE for the 6-phase induction generator in the disturbance-free case.

No test	$RMSE_{x1}$	$RMSE_{x2}$	$RMSE_{x3}$	$RMSE_{x4}$	$RMSE_{x5}$	$RMSE_{x6}$
$setpoint_1$	0.0013	0.0013	0.0025	0.0020	0.0026	0.0013
$setpoint_2$	0.0015	0.0006	0.0032	0.0025	0.0030	0.0027
$setpoint_3$	0.0015	0.0006	0.0027	0.0018	0.0028	0.0015
$setpoint_4$	0.0014	0.0016	0.0036	0.0032	0.0033	0.0037
$setpoint_5$	0.0015	0.0006	0.0027	0.0018	0.0028	0.0015
$setpoint_6$	0.0013	0.0015	0.0037	0.0036	0.0033	0.0041
$setpoint_7$	0.0014	0.0010	0.0035	0.0032	0.0031	0.0036
$setpoint_8$	0.0017	0.0005	0.0027	0.0025	0.0035	0.0027

Table 3 Tracking RMSE for the 6-phase induction generator under disturbances.

$\Delta a\%$	$RMSE_{x1}$	$RMSE_{x2}$	$RMSE_{x3}$	$RMSE_{x4}$	$RMSE_{x5}$	$RMSE_{x6}$
0%	0.0015	0.0006	0.0027	0.0018	0.0028	0.0015
10%	0.0019	0.0007	0.0026	0.0016	0.0028	0.0012
20%	0.0023	0.0008	0.0026	0.0014	0.0029	0.0010
30%	0.0027	0.0009	0.0025	0.0011	0.0030	0.0007
40%	0.0031	0.0010	0.0024	0.0009	0.0030	0.0004
50%	0.0035	0.0012	0.0023	0.0007	0.0031	0.0001
60%	0.0038	0.0013	0.0023	0.0005	0.0032	0.0001

Table 4 Estimation RMSE for the H-infinity Kalman Filter × 10^{-4}.

No test	$RMSE_{\hat{x}1}$	$RMSE_{\hat{x}2}$	$RMSE_{\hat{x}3}$	$RMSE_{\hat{x}4}$	$RMSE_{\hat{x}5}$	$RMSE_{\hat{x}6}$
$setpoint_1$	0.0183	0.0051	0.0112	0.1012	0.0136	0.0082
$setpoint_2$	0.0356	0.0051	0.0245	0.0580	0.0078	0.0048
$setpoint_3$	0.0367	0.0052	0.0225	0.0913	0.0163	0.0113
$setpoint_4$	0.0535	0.0050	0.0399	0.0758	0.0111	0.0087
$setpoint_5$	0.0378	0.0048	0.0228	0.0542	0.0095	0.0060
$setpoint_6$	0.0410	0.0053	0.0308	0.0652	0.0105	0.0091
$setpoint_7$	0.0593	0.0058	0.0425	0.1192	0.0153	0.0122
$setpoint_8$	0.0169	0.0052	0.0119	0.0481	0.1032	0.0944

Table 5 Convergence times (sec) for the 6-phase induction generator.

No test	Ts_{x1}	Ts_{x2}	Ts_{x3}	Ts_{x4}	Ts_{x5}	Ts_{x6}
$setpoint_1$	4.0	4.0	2.5	2.5	1.0	3.0
$setpoint_2$	3.5	4.0	2.5	2.5	1.0	3.0
$setpoint_3$	3.5	4.0	2.5	2.5	1.0	3.5
$setpoint_4$	3.5	4.0	3.0	2.5	1.0	3.5
$setpoint_5$	2.5	2.5	2.0	2.5	1.0	2.0
$setpoint_6$	3.5	4.0	2.5	2.5	1.0	3.5
$setpoint_7$	3.0	2.0	3.5	3.0	1.0	3.5
$setpoint_8$	3.0	4.0	2.5	2.5	1.0	2.5

The transient characteristics of the control method depend primarily on the gains and coefficients which appear in the method's algebraic Riccati equation of Eq. (84). Actually, for small values of gain r one achieves the elimination of the state vector's tracking error for all reference setpoints. Besides, for relatively high values of the diagonal elements of the positive semi-definite symmetric matrix Q one achieves fast convergence of the state variables to their setpoints. Finally, small values of ρ contribute to the robustness of the control method. The smallest value of ρ for which a valid solution of the above-noted Riccati equation can be achieved in the form of a positive-definite and symmetric

matrix *P*, is the one that gives to the control loop its maximum robustness. The proposed nonlinear optimal (H-infinity) control scheme exhibits global (and not local) stability properties. This can be distinguished in the simulation experiments because the state variables of the six-phase induction generator can track time-varying and abruptly changing setpoints and converge to these setpoints no matter what their initial conditions may be. The control method also ensures the optimized functioning of the 6-phase induction generator-based renewable energy system after minimizing the variations of the control inputs. This means that the functioning of the 6-phase induction generator under variable operating conditions can be achieved with a minimal dispersion of energy.

The proposed nonlinear optimal control method is novel compared to past attempts for solving the optimal control problem for nonlinear dynamical systems [39, 41]. Unlike past approaches, in the new nonlinear optimal control method linearization is performed around a temporary operating point which is defined by the present value of the system's state vector and by the last sampled value of the control inputs vector and not at points that belong to the desirable trajectory (setpoints). Besides, the Riccati equation used for computing the feedback gains of the controller is new, and so is the global stability proof for this control method. Compared to NMPC (Nonlinear Model Predictive Control) which is a popular approach for treating the optimal control problem in industry, the new nonlinear optimal (H-infinity) control scheme is of proven global stability and the convergence of its iterative search for the optimum does not depend on initial conditions and trials with multiple sets of controller parameters. Notably, the nonlinear optimal control method is applicable to a wider class of dynamical systems than approaches based on the solution of State Dependent Riccati Equations (SDRE). The SDRE approaches can be applied only to dynamical systems which can be transformed to the Linear Parameter Varying (LPV) form. Besides, the nonlinear optimal control method performs better than nonlinear optimal control schemes which use approximation of the solution of the Hamilton-Jacobi-Bellman equation by Galerkin series expansions. The stability properties of the Galerkin series expansion-based optimal control approaches are still unproven.

Compared to other nonlinear control methods that one could have considered for six-phase induction generators, the presented nonlinear optimal (H-infinity) control approach exhibits specific advantages.

(a) Comapred to global linearization-based control schemes (such as Lie-algebra-based control and flatness-based control), the nonlinear optimal control approach does not use complicated changes of state variables (diffeomorphims) and transformations of the system's state-space description. The computed control inputs are applied directly to the initial nonlinear state-space model of the six-phase induction generator without the intervention of inverse transformations and thus without coming against the risk of singularities.

(b) In comparison to Nonlinear Model Predictive Control (NMPC) and to classical Model Predictive Control (MPC) the global stability properties of the nonlinear optimal control method are ensured. It is known that the performance and convergence to optimum of the iterative search of NMPC depend on parameter values selection and on initialization (multiple shooting methods).

(c) Notably, the use of the nonlinear optimal control method is not constrained to dynamical systems with a specific state-space form (input-output linearized, canonical, strict feedback or other). For instance in sliding-mode control unless the system is written in the input-output linearized form there is no systematic procedure for defining sliding surfaces. Moreover, in

backstepping control unless the system is found in the strict-feedback (backstepping integral) form there is no standard procedure for computing the backstepping control signal.

(d) Compared to PID-type control, the nonlinear optimal control method is of proven global stability, does not rely on any heuristics for selecting the controller's feedback gains and has global stability properties not affected by any changes in the operating points. PID controllers' performance depends on empirical tuning, which is carried out around local operating points.

(e) Unlike multiple models-based feedback control, the nonlinear optimal control method relies on using one single linearization point and avoids the need for defining empirically multiple fixed points. It also needs to solve only one Riccati equation and does not come against the solution of LMIs. Consequently, the nonlinear optimal control method does not come against dimensionality issues due to an exponential growth of the parameters of the control problem. As a consequence, the method's computational complexity remains moderate.

8. Conclusions

The article has proposed a nonlinear optimal control method for the control problem of 6-phase dual-star induction generators (DSIGs). Such a type of multiphase power generator finds use in renewable energy systems (wind power units or marine/tidal power units) because of achieving improved power generation rates while also exhibiting resilience to harsh operating conditions. The double three-phase windings of the stator of a DSIG generator are connected to the main electricity grid through a pair of AC/DC converters. The DSIG remains functional and can keep providing the grid with electric power even if one or more phases are subject to faults. The state-space model of the 6-phase DSIG is proven to be differentially flat. To implement the proposed nonlinear optimal control method the dynamic model of the DSIG undergoes approximate linearization through first-order Taylor series expansion and the computation of the associated Jacobian matrices. The linearization process takes place at each sampling instance around a temporary operating point which is defined by the present value of the generator's state vector and by the last sampled value of the control inputs vector.

A stabilizing H-infinity feedback controller is designed for the approximately linearized model of the DSIG. This controller represents a min-max differential game taking place between (i) the control inputs of the generator which try to minimize a quadratic cost function of the state vector's tracking error (ii) the model uncertainty and exogenous perturbation terms which try to minimize this cost function. To select the feedback gains of the H-infinity controller, an algebraic Riccati equation has to be solved at each time step of the control algorithm. The global stability properties of the control method are proven through Lyapunov analysis. The fine performance of the nonlinear optimal control scheme has been further confirmed through simulation experiments. It has been shown that all state variables of the DSIG achieve fast and accurate tracking of reference setpoints. The variations of the control inputs remain small which signifies that energy dispersion is minimized in applying the proposed control method.

Unlike other control schemes (e.g., sliding-mode control or backstepping control) the nonlinear optimal control method can be used for a wide class of electric power generators without constraints about the state-space form and structure of such electric machines. As explained, the nonlinear optimal control method exhibits significant advantages (it avoids the complicated diffeomorphisms of Lie algebra-based control, the stability issues of Nonlinear Model Predictive Control and the

limitations of sliding-mode control and backstepping control about finding the system into a specific state-space form). There are no limitations to the application of the nonlinear optimal control method, as long as the designer of the control scheme is willing to undertake the individual computational stages that constitute this control algorithm (computation of the Jacobian matrices of the system at each sampling period and solution of the method's algebraic Riccati equation at each sampling interval). The continuation of this research work is concerned with applying the nonlinear optimal control method to more types of multi-phase power generators, with more phases or with permanent magnets.

Author Contributions

The significance of the contribution of each author in this research work is indicated by the order of his name's appearance in the list of authors**.**

Competing Interests

The authors have declared that no competing interests exist.

References

1. Safaeinejad A, Rahimi M. Control and performance analysis of grid-connected variable-speed wind turbine with dual stator-winding induction generator for the contribution of both stator windings in active power transmission. IET Renew Power Gener. 2020; 14: 2346-2358.
2. Pantea A, Yazidi A, Betin F, Taherzadeh M, Carrière S, Henao H, et al. Six-phase induction machine model for electrical fault simulation using the circuit-oriented method. IEEE Trans Industr Electron. 2015; 63: 494-503.
3. Seck A, Moreau L, Benkhoris MF, Machmoum M. Automatic generation of optimal phase currents for five-phase PMSGs control under open-phase conditions. Proceedings of IECON 2017-43rd Annual Conference of the IEEE Industrial Electronics Society; 2017 October 29-November 01; Beijing, China. Piscatvie, New Jersey, USA: IEEE.
4. Chatterjee S, Chatterjee S. A novel speed sensor-less vector control of dual stator induction machine with space vector advanced 9-zone hybrid PWM for grid-connected wind energy generation system. Electr Power Syst Res. 2018; 163: 174-195.
5. Guettab A, Boudjema Z, Bounadja E, Taleb R. Improved control scheme for a dual star induction generator integrated in a wind turbine system and open-phase fault mode. Energy Rep. 2022; 8: 6866-6875.
6. Zhang J, Houari A, Seck A, Moreau L, Machmoum M. Fault tolerant control of a double stator permanent magnet generator in tidal current energy system. Proceedings of 2016 IEEE International Conference on Industrial Technology (ICIT); 2016 March 14-17; Taipei, Taiwan. Piscatvie, New Jersey, USA: IEEE.
7. Amimeur H, Aouzellag D, Abdessemed R, Ghedamsi K. Sliding-mode control of a dual-stator induction generator for wind energy conversion systems. Electr Power Energy Syst. 2012; 42: 60-70.
8. Hamitouche K, Chekkal S, Amimeur H, Aouzellag D. A new control strategy of dual stator induction generator with power regulation. J Eur des Syst Autom. 2020; 59: 469-478.

9. Toledo S, Ayala M, Maqueda E, Gregor R, Renault A, Rivera M, et al. Active and reactive power control based on predictive voltage control in a six-phase generation system using modular matrix converters. Proceedings of 2020 IEEE International Conference on Industrial Technology (ICIT); 2020 February 26-28; Buenos Aires, Argentina. Piscatvie, New Jersey, USA: IEEE.
10. Lu H, Li J, Qu R, Ye D. Fault tolerant predictive current control with two-vector modulation for six-phase permanent magnet synchronous machine drives. IET Electr Power Appl. 2018; 12: 169-178.
11. Bouyahia O, Betin F, Yazidi A. Fault-tolerant variable structure control of a low-speed 6-phase induction generator. Proceedings of 2021 IEEE 13th International Symposium on Diagnostics for Electrical Machines, Power Electronics and Drives (SDEMPED); 2021 August 22-25; Dallas, TX, USA. Piscatvie, New Jersey, USA: IEEE.
12. Taherzadeh M, Carriere S, Betin F, Joorabian M, Kianinezhad R, Capolino GA. On-line observer modification of a six-phase induction generator in faulted mode. Proceedings of IECON 2016-42nd Annual Conference of the IEEE Industrial Electronics Society; 2016 October 24-27; Florence, Italy. Piscatvie, New Jersey, USA: IEEE.
13. Mishra NK, Husain Z, Khan MR. D, Q reference frames for the simulation of multiphase (six-phase) wound rotor induction generator driven by a wind turbine for disperse generation. IET Electr Power Appl. 2019; 13: 1823-1834.
14. Liu J, Yang GJ, Li Y, Gao HW, Su JY. Eliminating the third harmonic effect for six-phase permanent magnet synchronous generators in one-phase open mode. J Power Electr. 2014; 14: 92-104.
15. Nurwati T, Carrière S, Betin F, Capolino GA. A new model for six-phase induction generator. Proceedings of IECON 2019-45th Annual Conference of the IEEE Industrial Electronics Society; 2019 October 14-17; Lisbon, Portugal. Piscatvie, New Jersey, USA: IEEE.
16. Chinmaya KA, Singh GK. Modelling and experimental analysis of grid-connected induction generator for variable speed wind-energy conversion system. Electr Power Syst Res. 2019; 166: 151-162.
17. Yazidi A, Pantea A, Betin F, Carriere S, Henao H, Capolino GA. Six-phase induction machine model for simulation and control purposes. Proceedings of IECON 2014-40th Annual Conference of the IEEE Industrial Electronics Society; 2014 October 29-November 01; Dallas, TX, USA. Piscatvie, New Jersey, USA: IEEE.
18. Zhou S, Rong F, Sun W, Huang S, Wu Q. AC/AC grid connection of six-phase wind power generator based on enneagon MMC converter. Int J Electr Power Energy Syst. 2020; 118: 105810.
19. Verma V, Singh R, Gour R. ADSIG as Gen-Former providing three-port network for safe coupling of distribution feeders in addition to wind energy harvesting. Int J Electr Power Energy Syst. 2020; 117: 105573.
20. Che HS, Levi E, Jones M, Duran MJ, Hew WP, Rahim NA. Operation of a six-phase induction machine using series-connected machine-side converters. IEEE Trans Industr Electron. 2013; 61: 164-176.
21. Carrière S, Betin F, Capolino GA, Taherzadeh M, Joorabian M, Kianinezhad R. Robust control of a six-phase induction generator under open-phase fault conditions. Proceedings of 2016 IEEE 25th International Symposium on Industrial Electronics (ISIE); 2016 June 08-10; Santa Clara, CA, USA. Piscatvie, New Jersey, USA: IEEE.
22. Marouani K, Nounou K, Benbouzid M, Tabbache B, Alloui H. Control of a power generation system based on a dual star induction generator. Proceedings of ICREPQ'15, International

Conference on Renewable Energy Systems and Power Quality; 2015 March 25-27; La Coruña, Spain.
23. Taherzadeh M, Carriere S, Betin F, Joorabian M, Kianinezhad R, Capolino GA. Online controller modifying of a six-phase induction generator in phase opening occurrences. Proceedings of 2014 International Conference on Electrical Machines (ICEM); 2014 September 02-05; Berlin, Germany. Piscatvie, New Jersey, USA: IEEE.
24. Pantea A, Sivert A, Yazidi A, Betin F, Carriere S, Capolino GA. Efficient field-oriented control with power losses optimization of a six-phase induction generator for wind turbines. Proceedings of IECON 2016-42nd Annual Conference of the IEEE Industrial Electronics Society; 2016 October 23-26; Florence, Italy. Piscatvie, New Jersey, USA: IEEE.
25. Fnaiech MA, Betin F, Capolino GA. Sliding-mode control applied to the inner-loop regulation of a faulted six-phase induction machine (6 PIM). Proceedings of 2009 IEEE International Electric Machines and Drives Conference; 2009 May 03-06; Miami, FL, USA. Piscatvie, New Jersey, USA: IEEE.
26. Sari B, Benkhoris MF, Hamida MA, Chouaba SE. A backstepping torque control of a five-phase permanent magnet synchronous machine. Proceedings of 2018 7th International Conference on Systems and Control (ICSC); 2018 October 24-26; Valencia, Spain. Piscatvie, New Jersey, USA: IEEE.
27. Pantea A, Yazidi A, Betin F, Carriere S, Capolino GA. Simulation and experimental control of six-phase induction generator for wind turbines. Proceedings of 2016 XXII International Conference on Electrical Machines (ICEM); Lausanne, Switzerland. Piscatvie, New Jersey, USA: IEEE.
28. Wang S, Imai K, Doki S. A novel decoupling control scheme for non-salient multi-three-phase synchronous machines based on multi-stator model. IEEE Trans Ind Appl. 2022; 59: 886-896.
29. Bouyahia O, Betin F, Yazidi A. Fault tolerant variable structure control of six-phase induction generator for wind turbines. IEEE Trans Energy Convers. 2012; 37: 1579-1588.
30. Bouyahia O, Betin F, Yazidi A. Optimal sliding-mode control of a symmetrical six-phase indution generator for wind turbines. IEEE Trans Ind Appl. 2022; 58: 7308-7317.
31. Pantea A, Yazidi A, Betin F, Carrière S, Sivert A, Vacossin B, et al. Fault-tolerant control of a low-speed six-phase induction generator for wind turbines. IEEE Trans Ind Appl. 2018; 55: 426-436.
32. Chekkal S, Lahaçani NA, Aouzellag D, Ghedamsi K. Fuzzy logic control strategy of wind generator based on dual-stator induction generator. Int J Electr Power Energy Syst. 2014; 59: 166-175.
33. Fnaiech MA, Betin F, Capolino GA, Fnaiech F. Fuzzy and sliding-mode controls applied applied to six-phase induction machine with open phases. IEEE Trans Industr Electron. 2009; 57: 354-364.
34. Iqbal A, Singh GK. PSO-based controlled six-phase grid-connected induction generator for wind energy conversion. CES Trans Electr Mach Syst. 2021; 5: 41-49.
35. Rigatos G, Tzafestas S. Extended Kalman filtering for fuzzy modelling and multi-sensor fusion. Math Comput Model Dyn Syst. 2007; 13: 251-266.
36. Basseville M, Nikiforov I. Detection of abrupt changes: Theory and applications. Englewood Cliffs: Prentice Hall; 1993.
37. Rigatos G, Zhang Q. Fuzzy model validation using the local statistical approach. Fuzzy Sets Syst. 2009; 160: 882-904.
38. Rigatos G, Abbaszadeh M, Siano P. Control of dynamical nonlinear and partial differential equation systems: Theory and applications. London: IET Publications; 2022.

39. Rigatos GG. Nonlinear control and filtering using differential flatness approaches: Applications to electromechanical systems. Berlin, Germany: Springer; 2015.
40. Rigatos G. Intelligent renewable energy systems: Modelling and control. Berlin, Germany: Springer; 2016.
41. Rigatos G, Karapanou E. Advances in applied nonlinear optimal control. Newcastle upon Tyne, England: Cambridge Scholars Publishing; 2020.
42. Rigatos GG. Modelling and control for intelligent industrial systems. Adaptive algorithms in robotics and industrial engineering. Berlin, Germany: Springer; 2011.
43. Toussaint GJ, Basar T, Bullo F. H_∞ optimal tracking control techniques for nonlinear underactuated systems. Proceedings of the 39th IEEE Conference on Decision and Control (Cat. No.00CH37187); 2000 December 12-15; Sydney, NSW, Australia. Piscatvie, New Jersey, USA: IEEE.